Title
Morphological Characterization of M&#65533;ller Glial Mitochondria in Healthy and Degenerating Retina

Author
Nguyen, Thao Thi Thu

Publication Date
2020

Peer reviewed|Thesis/dissertation

UNIVERSITY OF CALIFORNIA

Los Angeles

Morphological Characterization of Müller Glial Mitochondria in Healthy and Degenerating Retina

A thesis submitted in partial satisfaction

of the requirements for the degree Master of Science

In Physiological Science

by

Thao Thi Thu Nguyen

2020

ABSTRACT OF THE THESIS

Morphological Characterization of Müller Glial Mitochondria
in Healthy and Degenerating Retina

by

Thao Thi Thu Nguyen

Master of Science in Physiological Science
University of California, Los Angeles, 2020
Professor Xianjie Yang, Co-Chair
Professor Patricia Emory Phelps, Co-Chair

Müller glial cells are derived from the same progenitor pool as retinal neurons during development, and their processes span the entire mature retina. Müller glial cells show similarities to astrocytes of the central nervous system and serve vital roles of maintaining homeostasis and integrity of the neural retina. In cold blood vertebrates, Müller glial cells act as endogenous stem cells to repair damaged retinas. In the brain, mitochondria were shown to influence axon branching, synaptic function, and neurogenesis. Many neurodegenerative diseases, such as Parkinson's, involve mitochondrial dysfunction. Recent research now focuses on the metabolic partnership between Müller glial cells and retinal neurons. However, the metabolic response of Müller glia to distress signals such as neural degeneration is

not well understood. This study combines advanced molecular genetic tools and super-resolution imaging technology to decipher Müller mitochondrial morphology and distribution within the integrated retinal neural network. The data show that the overall retinal health conditions, such as photoreceptor degeneration, influence the mitochondrial network of Müller glia. The Müller mitochondrial morphology of degenerating retina was significantly diverse throughout the cell length, and they are more elongated or tubular as compared with healthy retina in all retinal layers. These results contribute to our understanding of how Müller glial metabolism may impact neuronal function and survival.

The thesis of Thao Thi Thu Nguyen is approved.

David William Walker, Committee member

Patricia Emory Phelps, Committee Co-Chair

Xianjie Yang, Committee Co-Chair

University of California, Los Angeles

2020

DEDICATION

This thesis is dedicated to my family and, more particularly, my parents and my grandma for your unwavering support.

TABLE OF CONTENTS

LIST OF FIGURES

LIST OF TABLES

ACKNOWLEDGEMENTS

I wish to express my gratitude toward my mentor, Dr. Xian-Jie Yang, for the opportunity to join the lab and for your consistent guidance throughout my research.

I would like to thank my thesis committees, Dr. Patty Phelps and Dr. David Walker, for your time and insightful input throughout the process.

Very special thanks to the current and former members of Yang lab: Dr. Xiang-Mei Zhang, Dr. Kun Do Rhee, Dr. Yanjie Wang, and Lillian Lai, who have helped me develop my skill sets; Kevin Nguyen, Katie Pohl, Hong-Zhe Ma, and Joyce Xiong for your invaluable friendship and assistance.

I would like to thank Marisela Diaz-Vasquez: your expert counsels and academic planning keep me on track of other commitments beside research.

A warm thank you to my close friends and Terry, who have been there for me throughout my endeavors.

I would like to acknowledge the funding provided by the National Institute of Health and the Research to Prevent Blindness Foundation, Department of Ophthalmology at UCLA, for supporting this project.

INTRODUCTION

Organization of Neurons and Müller glial cells in the Retina.

As a constituent of the central nervous system (CNS), several major types of neurons and glial cells comprise the retina (Figure 1), which plays roles in detecting, processing, and transmitting visual information [1]. The retinal glia population includes resident microglia, brain-derived astrocytes, and the retina-specific Müller glia [2]. Developmentally, Müller glial cells share a linage with the six primary types of retinal neurons and are the last cell type to emerge and differentiate from multipotent retinal progenitor cells [3, 4]. Throughout retinogenesis, emerging neurons and glia organize their cell bodies into three nuclear layers and grow axonal and dendritic processes to form two synaptic layers. This laminar structure establishes retinal neural circuitry that enhances visual sensory signals [5-7].

As light enters the eye, the transparent cornea and lens facilitate light incidents to focus onto the retina at the inner surface of the eye. The rod and cone photoreceptors, with their cell bodies occupying the outer nuclear layers (ONL), employ photopigments embedded at their outer segments to detect light signals. Rod cells enable black and white vision in dim light (scotopic), and cone cells enable high-acuity color vision in bright light (photopic). Photoreceptors convert light signals into chemical signals and convey them to interneurons through synaptic connections at the outer plexiform layer (OPL). Bipolar cells localized in the inner nuclear layer (INL) are the central interneurons that relay visual signals from photoreceptors to retinal ganglion cells (RGCs) residing in the ganglion cell layer

(GCL). Bipolar cells form synaptic junctions with photoreceptors at the outer plexiform layer (OPL) and RGCs at the inner plexiform layer (IPL). Two other types of interneurons also integrate and regulate signals presented to RGCs. Horizontal cells positioned at the outer margin of the INL form synaptic connections with photoreceptors and bipolar cells within OPL, while amacrine cells localized along the inner portion of the INL synapse with bipolar cells and RGCs at IPL. RGCs project long axons that exit the eye to form the optic nerve to connect the retina with visual centers in the brain.

During the late stage of retinogenesis, Müller glial cells situate their cell body in the INL and extend a radial trunk that spans the entire thickness of the retina from the outer to the inner limiting membrane (OLM, ILM). As the retina continues to mature, Müller glial central trunk grows extensive processes into all retinal layers to surround neurons and blood vessels [8, 9]. Müller glial cells have heterogeneity in branching morphologies, which were proposed to reflect the specialized glia-neurons interactions in each retinal layer [10]. Even though the anatomy and spatial organization of Müller glial cells are described thoroughly [9], much remains unknown about the specific Müller glia-neuron interactions that support visual function.

Functional Interactions of Müller Glial Cells and Retinal Neurons.

Müller glial cells in the retina share functional similarities to astrocytes in the CNS [11] and play vital roles in the retina due to their unique morphologies. Even though most retinal neurons have reached their final positions before the terminal differentiation of Müller glia from progenitor cells [12], Müller glial cells provide a physical scaffold for retinal organization and serve important roles in retinal

development and survival. Induction of primary apoptosis in Müller glial cells of transgenic mice at postnatal (P) days 6 - 10 leads to abnormal development in retinal architecture, causing massive secondary photoreceptor cell death by P21, and results in outer retinal degeneration [13].

Mature Müller glial cells actively transcribe a large number of genes expressed by retinal progenitor cells, suggesting that they may reserve progenitor-like potentials [14]. Indeed, in the chick retina and certain cold-blooded vertebrates, such as amphibians and teleost fishes, Müller glial cells demonstrate the ability to act as endogenous stem cells and can revert back to a proliferative state and differentiate into neurons to repair injured retina [15-18]. Ongoing research has sought to stimulate similar stem cell potentials in Müller glia of mammalian retinas using approaches such as supplying growth factor cues or neurogenic transcription factors [18-22].

Müller glial cells also closely interact with retinal neurons to maintain the retina's homeostasis and provide physiological support for neuronal functions. While the retinal pigment epithelium (RPE) cells participate in the uptake and conversion of all-trans-retinol to 11-cis retinal required for phototransduction via the visual cycle, Müller glia facilitate this recycling process principally for cones [23, 24]. Additionally, Müller glial processes surround synaptic connections of neurons to modulate neurotransmitter release and contribute to neurotransmitter reuptake [25, 26] via glutamate aspartate transporter 1 (GLAST-1) or solute carrier family 1 member 3 (SLC1A3) in human [27, 28]. Müller glia is the only cell type in the retina that express glutamine synthetase (GS) that catalyzes the ATP-dependent reaction to synthesize glutamine from glutamate and ammonia, which then release

glutamine back to neurons for neurotransmitter recycling [29, 30]. Besides structural, regenerative, and physiological support, Müller glial cells also form a metabolic partnership with neurons to uphold the retinal metabolic demand [31].

Müller Glial Cell Metabolism and the Retinal Metabolic Demand.

Similar to astrocyte and neurons metabolic relationship in the CNS, some publications suggest that Müller glia utilize glycolysis for ATP production and provide neurons with lactate [32-34]. However, other evidence indicates that glia-neuron metabolic partnership leads to a low expression level of glycolytic enzyme—pyruvate kinase and a component of the malate-aspartate shuttle—aspartate/glutamate carriers in Müller glia, so Müller glia could not utilize the glycolytic pathway and glutamate directly for energy production [35]. Instead, Müller glial cells may mainly use the glycolytic product lactate from neurons as fuel [36]. Other in vitro studies using dissociated Müller glia showed that Müller could increase their glycolysis rate or rely on the TCA cycle to produce ATP in metabolically stressful conditions such as anoxia or low glucose [31, 37]. These results might suggest that Müller glial cells have the capability to change and adapt their metabolic activities to sustain the retina.

The retina has one of the highest demands for oxygen consumption in the body, and visual function is susceptible to hypoxia [38, 39]. The effect of depleted oxygen on anoxia-tolerant vertebrates shows the reduction of the amplitude of electroretinogram, especially the b-wave, which measures the functionality of the inner retina (predominantly ON-bipolar cells) [40]. The high metabolic needs are due to the ion transport in neurons, which actively pump ions against their concentration gradients with the cost of ATP to maintain the neuronal membrane's

potential. Insufficiencies in energy metabolism, such as oxidative stress and mitochondrial dysfunction, can lead to visual deficits, degenerative retinal diseases, and eventually blindness [41, 42].

Outer Retinal Degenerative Disease and Müller Glial Cells in Pathological Conditions.

Retinitis pigmentosa (RP) is one of the most common hereditary eye diseases of the retina associated with vision loss due to photoreceptor cell death via apoptosis, with an estimated prevalence between 1 in 2500 to 1 in 7000 people [43]. RP frequently occurs with an initial degeneration of rod photoreceptors, followed by the death of cone cells [44, 45]. Generally, RP patients exhibit early symptoms of impairment of dark adaptation and night blindness during adolescence. The patients then suffer from reduced peripheral vision during early adulthood, which over time, leads to tunnel vision and eventually loss of central vision by age 60 [45]. The clinical examination of the human fundus shows attenuation of the retinal arterioles and a trademark “black clumping” (bone spicules pigmentation) near the retinal vessel due to epithelial pigment leaking into the retina [46, 47].

Genetically, most RP cases are due to single-gene mutations that are mainly expressed in rods. To date, 22 autosomal dominant, 41 autosomal recessives, and 2 X-linked RP genes have been identified and listed in the RetNet database (https://sph.uth.edu/RetNet/sum-dis.htm). The most common functions of the mutated genes in rods include components of the phototransduction cascade (rhodopsin, phosphodiesterase), disc membrane-associated glycoproteins (peripherin2), and the light-sensitive cationic channels [48, 49]. However, the

mechanisms of these mutations leading to the death of rods and secondary cone cells death are often not clear.

It was proposed that cones need survival factors released by rods, and that the rod support towards cone viability is linked to glucose availability and aerobic glycolysis [50, 51]. Recent studies also revealed that mouse photoreceptors employ the glycolytic enzyme pyruvate kinase M2 isoform and aerobic glycolysis to meet the anabolic demands for outer segment biogenesis and outer retina health [36, 52-54]. Other postulated causes of secondary cones degeneration include oxidative stress and metabolic impairment [55].

With the current understanding of RP, numerous treatment strategies are being developed to slow the rate of disease progression. Because many gene mutations can be involved in RP, currently there is no general cure available for retinal degeneration. The existing clinical trials for RP and other retinal diseases involve the potent neuroprotective agent Ciliary neurotrophic factor (CNTF), and previous work has shown that Müller glial cells are among the first cell type in the retina that responds to neuroprotective signals [56]. In pathological conditions, Müller glial cells become reactive (gliosis) and upregulate the expression of the glial fibrillary acidic protein (GFAP) [57]. In degenerating retina, Müller glial cells adapt a heterogeneity of metabolic phenotypes compared with a consistent metabolic profile in a healthy retina [58]. The underlying reasons that lead to these changes are still unclear; however, these introduced works indicate the importance of metabolic homeostasis in both retinal neurons and glia for normal function and neuronal survival.

Mitochondria in Müller Glial Cells and Proposed Study.

Mitochondria are dynamic organelles and have long been acknowledged for their primary function as ATP production sites in eukaryotic cells through oxidative phosphorylation (OXPHOS). Recently, studies reported that mitochondria also interact with other cellular organelles to regulate cellular metabolic homeostasis and survival [59, 60]. Current studies in the brain revealed the influence of mitochondria on axon branching, synaptic function, and neurogenesis [61]. Major neurodegenerative diseases, such as Parkinson's, involve mitochondrial dysfunction [62-64]. Accumulating evidence also indicates that cellular metabolic status is closely related to stem cell potentials, neural repair, and regeneration. It is especially important to further the understanding of CNS glial metabolism and how it influences neuronal function and survival.

This study aims to characterize mitochondrial morphology and distribution in Müller glia and to test whether they are influenced by neurons in various retinal layers and overall retinal health conditions. Since Müller glia have extensive processes throughout the retinal neural network, it has been challenging to elucidate the mitochondrial morphology, distribution, and dynamics of Müller cells. Previous transmission electron microscopy (TEM) studies found highly concentrated mitochondria at distal ends of Müller processes by the outer and inner limiting membranes [65, 66]. However, the current knowledge about Müller mitochondrial functions and their metabolic interaction with retinal neurons is limited [29].

In this thesis study, I used advanced molecular genetic tools to specifically label Müller mitochondria in the mouse retina, and to reveal the mitochondrial morphology and distribution of a single Müller glial cell and the entire Müller

population within an integrated neural network. In addition, I applied super-resolution imaging using structured illumination microscopy (SIM) to capture images of Müller mitochondria in both wild type and a mouse model of RP and performed computational analyses to reveal the changes of the Müller mitochondrial network in healthy and degenerating retinas. The results of this study provide a foundation for future investigations of how Müller glial metabolism may impact retinal neuronal function and survival.

MATERIALS AND METHODS

Animals.

The *GLAST-creER* [JAX #012586] [67], *PhAM floxed* [JAX #18385] [68], and *Ai14* reporter [JAX #007914] [69] mouse lines were previously described and obtained from the Jackson Laboratory. The *rds/Peripherin2 P216L* transgenic mice (*Rds*) were generated by the Travis lab [70]. All mouse lines had *C57B6/J* background originally and were backcrossed to the *WT CD1* background (Charles River #022) for at least two generations. For experimentation, the Cre driver with the genotype *GLAST-creER; Rds; PhAM*$^{fl/fl}$ was established. The Driver mouse was crossed with the Cre reporter line *Ai14*$^{fl/fl}$. This cross produced F1 generation that all carry one copy of *Ai14* and *PhAM* to label Müller glial cells and their mitochondria in a Cre-dependent manner, in either *WT* or *Rds* background. Mice were maintained under standard housing conditions on a 12-hour light/12-hour dark cycle with food and water ad libitum. The experimental analyses included both female and male mice from the same litter or with age-matched controls. All animal procedures followed the *National Institutes of Health Guide for the Care and Use of Laboratory Animals, Eighth Edition* (National Institutes of Health Publication, revised 2011) and were approved by the Animal Research Committee at the University of California, Los Angeles.

Genotyping.

Tail biopsy samples were collected from all F1 progeny between postnatal days 10-12 (P10 – P12). Genotypes for individuals were determined by polymerase chain reaction (PCR) using genomic DNAs and the following primers: *Cre* (forward:

GAC GAT GCA ACG AGT GAT GA, reverse: AGC ATT GCT GTC ACT TGG TC); *Rds* (forward: CCT GGA GTT GCG CTG T, reverse: GTC TTT TTC ATG AAG CAC C); *PhAM* (primer 1: CCA AAG TCG CTC TGA GTT GTT ATC, primer 2: GAG CGG GAG AAA TGG ATA TG, primer 3: TCA ATG GGC GGG GGT CGT T); *Ai14* (primer 1: AAG GGA GCT GCA GTG GAG TA; primer 2: CCG AAA ATC TGT GGG AAG TC; primer 3: GGC ATT AAA GCA GCG TAT CC; primer 4: CTG TTC CTG TAC GGC ATG G)

CreER Induction by Tamoxifen.

Tamoxifen (Sigma-Aldrich, T5648) was dissolved in coin oil through vortexing at 37 degrees Celsius (°C) for 45 to 60 minutes to make either a 50 mg/mL or 12.5 mg/mL solution. To obtain maximum induction (dense labeling) of Müller glial cells, Tamoxifen (50 mg/mL) solution was injected into the peritoneal cavity of mice (IP injection) at P12, P13, P14 with a dose at 0.2 mg/g body weight. To achieve sparsely labeled Müller glia, P21 mice had tamoxifen (12.5 mg/mL) treatment once by IP injection with 0.05 mg/g dosage.

Tissue Preparation.

Mice were put under deep anesthesia with isoflurane (NDC: 60307-120-25) and euthanized by cardiac perfusion with 4% paraformaldehyde (PFA, Sigma-Aldrich, 158127) in phosphate buffer saline (PBS). The eyes were enucleated and incised along the ora serrata to remove the cornea and the lens, resulting in optic cups.

For experiments using retinal cross-sections, the optic cups containing the retina were fixed in 4% PFA/PBS for 2 hours at 4°C. After three quick washes with PBS to remove residual PFA, the eyecups were submerged in 30% sucrose/PBS for cryoprotection overnight at 4 °C, then exchanged into a 1:1 mixture of 30%

sucrose and optimal cutting temperature compound (OCT, Sakura Finetek, 4583), followed by embedding into OCT blocks. The tissue blocks were stored at -20 °C or -80 °C until being sectioned on a cryostat (CryoStar NX50, Thermo Fisher). The 20 - 50 μm thickness tissues were collected on glass slides (Fisher, 12-550-15) and stored in a dark box without moisture at -20 °C.

For experiments using flat-mounted tissues, the retinas were isolated from the eyecups and fixed in 4% PFA/PBS for 2 hours at 4°C. After three quick washes in PBS, the retinas were submerged in sterile PBS until imaging analysis.

Immunohistochemistry.

For nuclear DNA staining, retinal cross-section slides were washed with PBS and incubated with 4’,6-diamidino-2-phenylindole (DAPI, Sigma-Alrich, D9542) in PBS (1:500 dilution) for 20 minutes. Three more final washes in PBS with 5 minutes intervals to remove any residual background. Similarly, the whole retinas were incubated with DAPI in PBS (1:300) for 48 hours and followed by extensive washes to remove any excessive background.

For immunolabeling with antibodies, the slides were washed with PBS and incubated at room temperature in a blocking solution (DMEM with 10% fetal bovine serum, 0.1% Triton X-100, 1% Donkey serum in PBS) for 2 hours. The slides were then incubated with primary antibodies at 4 °C overnight and with secondary antibodies and DAPI at room temperature for 2 hours. Each antibody incubation was followed by three 30 minutes washes of PBS. The antibodies used are summarized in Table 1.

The slides with retinal sections were mounted in antifade mounting medium (Vectashield Rf 1.45, Vector laboratories) with #1.5 coverslips (0.16 – 0.19 mm,

Thermofisher). To maximizing SIM imaging quality, flattened whole retinas were mounted onto the #1.5 coverslips, instead of glass slides, with either the retinal ganglion cell layer or the photoreceptors layer directly touching the coverslip. The coverslips were then sealed to glass slides with coverslip sealant (CoveGrip, biotium, 23005) and allowed to dry in a dark chamber at room temperature.

Confocal and Structured Illumination Microscopy (SIM) Imaging.

Confocal images were captured on an inverted fluorescence microscopy (Olympus IX81) with UPLFLN 40x/1.3 NA oil objective. Images were acquired using FluoView 1000 software (Olympus) with a Z-spacing of 1 μm.

Super-resolution cross section and flat-mount images using Structured Illumination Microscopy (SIM) were captured on the Deltavision 3D-SIM OMX system (GE Healthcare) with PlanApoN 60x/1.42 NA oil objective (Olympus). Images were acquired in 3D structured illumination mode using a Z-spacing of 0.125 μm and reconstructed using Softworx software (GE Healthcare).

Mitochondrial Morphology Analysis.

SIM images were analyzed in FIJI/ImageJ [71] using the open-source software plugin MitoMap (accessible at http://www.gurdon.cam.ac.uk/stafflinks/downloadspublic/imaging-plugins) [72]. The plugin automates the process to compute mitochondrial volume (μm^3), surface area (μm^2), and other geometrical features in a region of interest (ROI). The parameters' details are listed in Table 2. For each sample analysis, the 32-bit OMX images stack (dv file) are loaded onto ImageJ using the Bio-formats plugin [73], and an ROI was chosen that includes the center 1000x1000 pixels (40 x 40 um) region (OLM region) or contain a region of a single cell (ONL, INL, RGC regions

across the retina). The MitoMap plugins converted the images stack to 16-bit and applied Otsu thresholding [74] to extract the PhAM reporter-labeled mitochondrial volume. MitoMap applied several mathematical formulas to the obtained volume to quantify the geometrical features. The details of the equations and validity of the method can be referred back to the developer's publication [72]. Before the analysis, objects with a volume smaller than 0.1 μm^3 were excluded to eliminate artifacts.

Statistical Analyses.

For all of the statistical analyses on mitochondrial morphology between *WT* and *Rds* retina, the Mann-Whitney U test was employed because the assumptions of the independent samples t-test are violated (non-parametric), and values of $P < 0.05$ were considered statistically significant. The statistical tests were done on the JASP program [75]. The principal component analyses were performed on R Studio using 'factoextra' and 'FactoMineR' packages [76]. Data were plotted using R Studio 'ggplot2' and 'ggbiplot' packages [77].

RESULTS

Genetic Labeling of Müller Glial Mitochondria in Healthy and Degenerating Retinas.

In this study, I aim to characterize Müller glial mitochondria using molecular genetic approaches in both healthy and diseased mouse retinas. To model retinal degeneration, I chose the retinal degeneration slow (*Rds*) mouse carrying the *Peripherin2 (Prph2) P216L* mutant transgene (referred to as *Rds P216L* thereafter) [70]. *Prph2* encodes a structural protein located to the photoreceptor outer segment rim. The human *PRPH2* P216L mutation causes dominant RP with rod degeneration preceding the cone cell loss, which is mimicked in the *Rds P216L* transgenic mouse. To illustrate the Müller cells' location and the degeneration process in *Rds* retina, Müller glial markers were used to immunolabel the *WT* and *Rds* mutant retinas (Figure 2). At postnatal day 33 (P33), the *Rds* retina had 53% of photoreceptor nuclei remaining in the outer nuclear layer with shorter inner and outer segments as compared to the *WT* retina (Figure 2A, C). In both *Rds* and *WT* retinas, immunostaining by Sox9 and GS showed a row of Müller cell nuclei in the middle of the inner nuclear layer with GS-labeled processes spanning the entire retina (Figure 2B, D).

In order to achieve Cre-dependent gene activation in retinal Müller glia, a transgenic mouse with GLAST (Slc1a3) promoter-driving CreER was used [67]. The CreER recombinase consists of Cre fused to a mutated ligand-binding domain of the estrogen receptor (ER) and can be induced upon ligand binding to enter the nucleus. To test the specificity of the inducible CreER-mediated recombination,

GLAST-CreER mouse was crossed with the *Ai14*$^{fl/fl}$ mouse line, which expresses the tdTomato fluorescence protein in a Cre-dependent manner [69] (Figure 3A, B). When exposed to an estrogen analog such as Tamoxifen (Tm), the CreER expressing cells are expected to express tdTomato. Following IP injections of Tm (Figure 3C), tdTomato reporter was detected specifically in Müller glial cells in CreER+ retinas 5 days after treatment, whereas Cre- retina showed no detectable reporter signals (Figure 3D, E). This data indicated the Tm induction scheme used can result in Müller glial specific Cre activation.

To image Muller glial mitochondria, the *PhAM* mouse that expresses the Dendra2 fluorescent reporter with an n-ternimal mitochondrial targeting sequence was used [68]. To test the mitochondrial labeling, genetic crosses were performed to obtain mice that carry both *Ai14* and *PhAM* reporters (Figure 4A, B). After crossing with *GLAST-CreER* and Tm induction, *PhAM* reporter (green)-labeled mitochondria were detected in corresponded to tdTomato-labeled Müller glia (Figure 4C, D). Thus, induced *PhAM*-labeled mitochondria are specific to Müller glial cells and can be observed throughout the entire length of Müller glia with highly distributed mitochondria at the end-feet (Figure 4E).

Since Müller glial processes are densely distributed throughout the retina, it is necessary to achieve sparse labeling to enable visualization of individual Müller glial cells and their mitochondria. Therefore, the dosage and time of Tm induction were adjusted to achieve sparse *PhAM*-labeling. The Cre driver mouse with the genotype of *GLAST-CreER*; *Rds*; *PhAM*$^{fl/fl}$ were crossed to a *WT* mouse to assess Müller glial mitochondria in both *WT* and *Rds* backgrounds (Figure 5A top). With a high dose of Tm (0.2 mg/g) and early triple induction starting at P12 (Figure 5A

bottom left), the induction of *PhAM* occurred in the entire Müller glial population (Figure 5B, C). With a low dose of Tm (0.05 mg/g) and a later single induction at P21 (Figure 5A bottom right), sparse Müller glial cells labeling was achieved with mitochondria from individual Müller glia unveiled (Figure 5E, F). However, at the resolution of conventional scanning laser confocal microscopy, the mitochondrial morphology within Müller glial cells could not be captured with confidence, and the mitochondrial morphological differences in *WT* and *Rds* retinas could not be objectively quantified.

Super-resolution Imaging of Müller Mitochondria in *WT* and *Rds* Retinas.

To assess the mitochondrial morphology in Müller glia, a super-resolution imaging technology structured illumination microscopy (SIM) was applied. Depending on the sample conditions, SIM can achieve the resolution of 120 nanometers in XY and 340 nanometers in Z [72] (GE Health), which is more suitable for analyzing subcellular organelles such as mitochondrion. SIM images of retinal cross-sections showed while *WT* Müller glial cells have a population of similar mitochondria throughout the entire cell length (Figure 6A), *Rds* retina presented more heterogeneity in Müller mitochondrial morphology across retinal layers (Figure 6B), suggesting that the mitochondrial morphology of Müller glia may vary depending on the location within the retina.

Based on these observations and the association of Müller glia with distinct retinal neurons at each retinal layer, the SIM imaging and analyses were conducted in four sections of the neural retina using cross section and flat mount preparations: the outer limiting membrane (OLM), the outer nuclear layer (ONL), the inner nuclear layer (INL), and the retinal ganglion cell layer (GCL).

Müller Glial Mitochondria at the OLM.

Photoreceptors and Müller glial cells form adherens junctional complexes at the base of rods and cones inner segments that comprise the OLM, which creates a barrier regulating what molecules could enter the intercellular space in the retina [78]. The perturbation of OLM has been associated with RP [79, 80] and abnormal retinal development [81]. To compare Müller mitochondria at the OLM of *WT* and *Rds* retinas, F1 progenies of driver mouse with *GLAST-CreER; Rds; PhAM*$^{fl/fl}$ and *Ai14*$^{fl/fl}$ were induced with a high Tm dose at P12 to label all Müller glia and their mitochondria. Flat mount retinas were imaged en face from the photoreceptor side (Figure 7). The signals of DAPI and *Ai14* were used as landmarks to capture SIM images of the Müller mitochondria at the OLM of flat-mounted retinas. In the *WT* retina at P64, Müller mitochondrial population at the OLM consisted of small granular mitochondria (Figure 7A), and they formed a strict layer at the outer limiting membrane as indicated by the cross-sectional view (Figure 7B). *Rds* Müller glial processes at the OLM also had small size mitochondria but distributed more sparsely (Figure 7D). From the cross-sectional view, *Ai14* signals showed the abnormal sprouting of the *Rds* Müller processes, and the mitochondria morphology was more elongated compared to *WT* (Figure 7E vs. B). From the en face view of merged SIM images (1 μm), *Rds* Müller terminal processes also occupied a larger area (Figure 7F) as compared with *WT* (Figure 7C). It appeared that the *WT* mitochondria tended to cluster together and followed the circular shape of *WT* Müller processes labeled by tdTomato (Figure 7C).

The MitoMap analysis that allows quantification of mitochondrial morphological features was applied to the OLM region. These MitoMap features are listed in Table 2 [72]. A 40x40 μm in XY of SIM 5 μm Z-stacks were evaluated for the mitochondrial morphology between the *WT* and *Rds* (Figure 8). In the principal component analysis (PCA), six of the calculated featured from MitoMap separated mitochondria from *WT* and *Rds* retina into two groups with some significant differences (Figure 8A). The main separation along the first principal component (PCA1) was driven by surface area and volume. *WT* Müller glial cells contain a subpopulation of mitochondria slightly larger in size, but the differences were not significant (Table 3-A and 3-B). The surface area versus volume ratio (SA:V), compactness, and sphericity drove the separation in the second principal component (PCA2), with *Rds* Müller mitochondria have higher SA:V and lower sphericity (Figure 8B, C, Table 3-B). These quantitative terms agreed with the observation from SIM images (Figure 7B vs. 7E) that, even though both populations consisted of small-size mitochondria, *Rds* Müller mitochondria at the OLM were more elongated and less circular as compared to *WT*.

Müller Glial Mitochondria in the Outer Retina.

The degeneration of ONL is a hallmark of RP, and it is important to further understand the response of Müller glial cells to the degeneration of photoreceptors [57, 82]. To characterize the impact of *Rds P216L* on Müller mitochondria in the ONL, F1 progenies of the *GLAST-CreER; Rds; PhAM*$^{fl/fl}$ driver and *WT* were induced with a high Tm dose for full Müller induction and a low Tm dose for sparse induction. In retinal cross-sections at P60, *Rds* Müller mitochondrial network displayed a branched and tubular morphology (Figure 9C, D) compared to the *WT*

(Figure 9A, B). Similarly, in the volume view of a single Müller cell captured from flat-mount retinas at P114, *Rds* Müller contained an elongated and connected mitochondrion in addition to some small fragmented ones (Figure 9D), whereas *WT* Müller mitochondria were more fragmental (Figure 9B).

In PCA analysis, the main separation along the PCA1 was driven by surface area, volume, and sphericity (Figure 10A). The *WT* Müller mitochondrial morphology was significantly more spherical (Figure 10C) and have lower value in average volume and surface area (Table 4-B). The SA:V and compactness drove the separation in PCA2, and *Rds* Müller mitochondria have a higher value in compactness (Figure 10B, Table 4-B). The visual observation and quantitative analysis showed *Rds* Müller mitochondria in the ONL are larger and more elongated as compared with *WT*.

Responses of Müller mitochondria in the inner nuclear layer

Even though *Rds* mutant is a model for outer retinal degeneration, the Müller mitochondrial change was also observed in the inner retina. *WT* and *Rds* Müller glial in the INL contain a mixed mitochondrial population (Figure 11A, B). *Rds* Müller mitochondria had higher average volume, surface area, and sphericity (Table 5-B, Figure 11F), which were the main contributions to PCA1 (Figure 11C). The SA:V and distribution isotropy drove the separation in PCA2, with *Rds* Müller mitochondria have lower value in distribution isotropy, SA:V, and higher value in compactness (Figure 11 D, G, E). Based on quantitative terms and visual observation, *Rds* Müller mitochondria were larger and more tubular, while *WT* Müller glia had an asymmetrical interconnected network of mitochondria within the INL.

Müller Mitochondria in the Ganglion Cell Layer and the End-feet.

Müller glial end-feet surround the RGCs and their axons. Both *WT* and *Rds* Müller glial end-feet contain mitochondria with granular appearance (Figure 12 A, E). *Rds* mitochondria appeared larger compared to *WT* from the flat-mounted views (Figure 12B, F). The volume view of mitochondria from single Müller end-foot of flat-mounted retinas showed accumulation of mitochondria at the end-feet, and *Rds* Müller end-feet appeared to contain more mitochondria than *WT* (Figure 12C, D vs. G, H) (data were not quantified in this study). In PCA (Figure 13A), the main separation along the PCA1 was driven by surface area, volume, and sphericity. The differences in these values are not significant (Table 6-A). The SA:V, compactness and distribution isotropy drove the separation in PCA2, with *Rds* Müller glia have a higher value in mitochondrial compactness and lower value in distribution isotropy (Figure 13B, C, Table 6-B). Thus, *Rds* mitochondria at Müller end-feet were more tubular and rotationally symmetrical as compared to *WT*.

DISCUSSION

Müller glial cells have an intricate network of processes associated with retinal layers and specific synaptic sub-laminae [9]. The spatial specializations in Müller glial structure were proposed to act in synchrony with retinal neurons and support retinal physiology. This study characterized the morphology and distribution of Müller glial mitochondria in the healthy retina and showed that the overall retinal health conditions influence them. The investigative approaches used in this study had advantages over the conventional TEM because the combined technology of molecular genetic tools and super-resolution imaging allows elucidation of Müller mitochondrial morphology within an integrated neural network. In both healthy and degenerating retinas, individual Müller cells contain mitochondria throughout their entire radial length, but their distribution is more concentrated at specific retinal layers. Remarkably, the Müller mitochondrial morphology of *Rds* retina was significantly diverse throughout the cell length, and they are more elongated or tubular as compared with *WT* retina in all retinal layers (Figure 6A and B). It is interesting that photoreceptors degeneration could have a noticeable influence on Müller mitochondrial morphology throughout the retina.

Mitochondrial biogenesis, dynamics, and mitophagy comprise mitochondrial quality control to sustain functional cellular mitochondria [83]. Mitochondrial dynamics were linked to the balance between cellular metabolic demands and nutrient supply by favoring either connected or fragmented mitochondrial morphologies through fusion and fission. Mitochondrial elongation is described in physiological processes associated with starvation, acute stress, G1/S phase, and increase ATP synthesis coupled with respiration. The mitochondrial architecture

was shown to become more fragmented in an environment with excessive nutrients and associated with decreased coupling [84]. The drastic response of *Rds* Müller mitochondrial morphology toward elongation could reflect the alteration in metabolic profile across the Müller glial cells population [58, 85] along with the change in metabolism of the whole retina (unpublished work from Yang lab).

Photoreceptor cells in the retina show a very high metabolic rate as both maintaining the dark current and the active turnover of the outer segments where the photopigments concentrate require high energy consumption [36, 52-54, 86]. The disorganized and shorter outer segment of photoreceptors are hallmark phenotypes of RP [56, 87]. Without the normal architecture of the outer segment to house sufficient visual pigments, the phototransduction cascade in photoreceptors might not initiate efficiently in light. As the disease progressed with disrupted outer segments and loss of rod photoreceptors, the physiological processes, including dark adaptation and photon absorption, are affected. Reportedly, cones are metabolically more costly than rod cells, and the retina is more metabolically demanding in the dark than in exposed to light [86, 88-91]. The metabolism of Müller glial is also influenced by dark adaptation. In the mammalian retina, glycogen storage and glycogen phosphorylase are localized in Müller glial cells [92, 93], and ex vivo experiments had shown that the amount of glycogen decreases by 50% when the retina was transferred from light to darkness [94]. Since the high energy demand of *Rds* retina with a severe phenotype could be associated with dark adaptation, Müller mitochondria of *Rds* retina could deviate toward an elongated morphology as the results shown. Future analyses on young *Rds* mice

with an intact ONL and outer segment or dark-adapted *WT* mice could further test this hypothesis.

The retinal nutrient and oxygen sources could explain the subcellular mitochondrial heterogeneity of *Rds* Müller glial cells from the outer retina to the inner retina. Blood travels to the eye through the ophthalmic artery, which branches into two sources to supply the retina. The ciliary arteries become choroidal capillaries, which support the photoreceptors of the outer retina whereas the central retinal artery nourishes the inner retina [95]. Due to the different nutrient source, Müller mitochondria closer to the central retinal artery, such as in the IPL and GCL, would be experience less metabolic stress and would not show a significant change toward elongated morphology that is observed in *Rds* retina (Figure 6B, Figure 12E and F). Conditions that induce stress to the inner retina, such as NMDA-induced RGCs apoptosis or inner retinal disease mouse model, could be used to test this speculation and to determine its influence on Müller mitochondria.

WT and *Rds* Müller end-feet at the GCL accumulate a remarkable number of mitochondria with fragmental morphology. The *Rds* Müller mitochondria showed significantly more tubular and rotationally symmetrical morphology (Figure 12B and F). Mitochondrial fission that results in fragmented mitochondria facilitates the mitophagy process to eliminate damaged mitochondria and reduce oxidative stress. Impaired mitochondria that are not appropriately removed by mitophagy could lead to the accumulation of reactive oxygen species and various pathologies [96]. Alternately, *WT* Müller glia could be more active in fusion and fission processes and mitophagy that results in non-tubular and asymmetrical mitochondria architecture.

From this observation, further investigation could assess the mitochondrial dynamics and mitophagy machinery components in Müller glia and the mitochondrial functionality of these fragmented mitochondria.

Müller glial cells are postmitotic cells that retain expression of the cell cycle G1/S phase promoting Cyclin D3 and have regenerative potential. Shortly after damage to the mammalian retina, Müller glial cells turn off the cyclin kinase inhibitor p27KIP1 and increase Cyclin D1 expression to drive a brief period of S-phase [97-99], but they will not proliferate and differentiate into retinal neurons without further stimulations. During the G1/S phase of the cell cycle, a large increase in energy demand to support biogenic processes lead to mitochondrial elongation [100, 101]. The damage signals from *Rds* retina could drive Müller glia to become reactive and enter G1/S phase. As observed with elongated mitochondrial phenotype, Müller glial cells are speculated to retain high mitochondria fusion levels to accommodate the metabolic demand from photoreceptors degeneration and biogenic processes. Mitochondrial dynamics has been shown to regulate neurogenesis and influence fate decision in postmitotic cortical cells [102]. Increased mitochondria fission promotes neuronal fate decisions, but mitochondria fusion induction redirects postmitotic cells toward self-renewal. Thus, the high levels of mitochondria fusion would impede the potential for *Rds* Müller glial cells to differentiate into neurons and repair the retina. In addition, it was suggested that depletion of mitochondria fusion leads to inactivation of the Hippo pathway [103], and the deletion of the Hippo pathway could drive mammalian Müller glial cells proliferation spontaneously in the absence of retinal damage [99]. Based on these observations, the regenerative potential of

mammalian Müller glial cells could be modulated by temporarily suppressing mitochondria fusion or induce fission in *WT* and *Rds* retina. Alternatively, it is possible that altered mitochondrial morphology reflects the change of Müller glial cell metabolic status, which may impinge on their proliferative and regenerative potentials.

Together, the results presented in this thesis provided a comprehensive representation of Müller mitochondrial morphology and distribution in healthy and photoreceptor degenerating conditions. This study lays a foundation for further investigations on how glia-neuron metabolic interactions may impact retinal physiology, neuronal survival, and retinal repair. Future research of mitochondria dynamics and activity in Müller glial cells or within specific cell types of an integrated neural network may facilitate the development of effective cellular metabolism-based therapies.

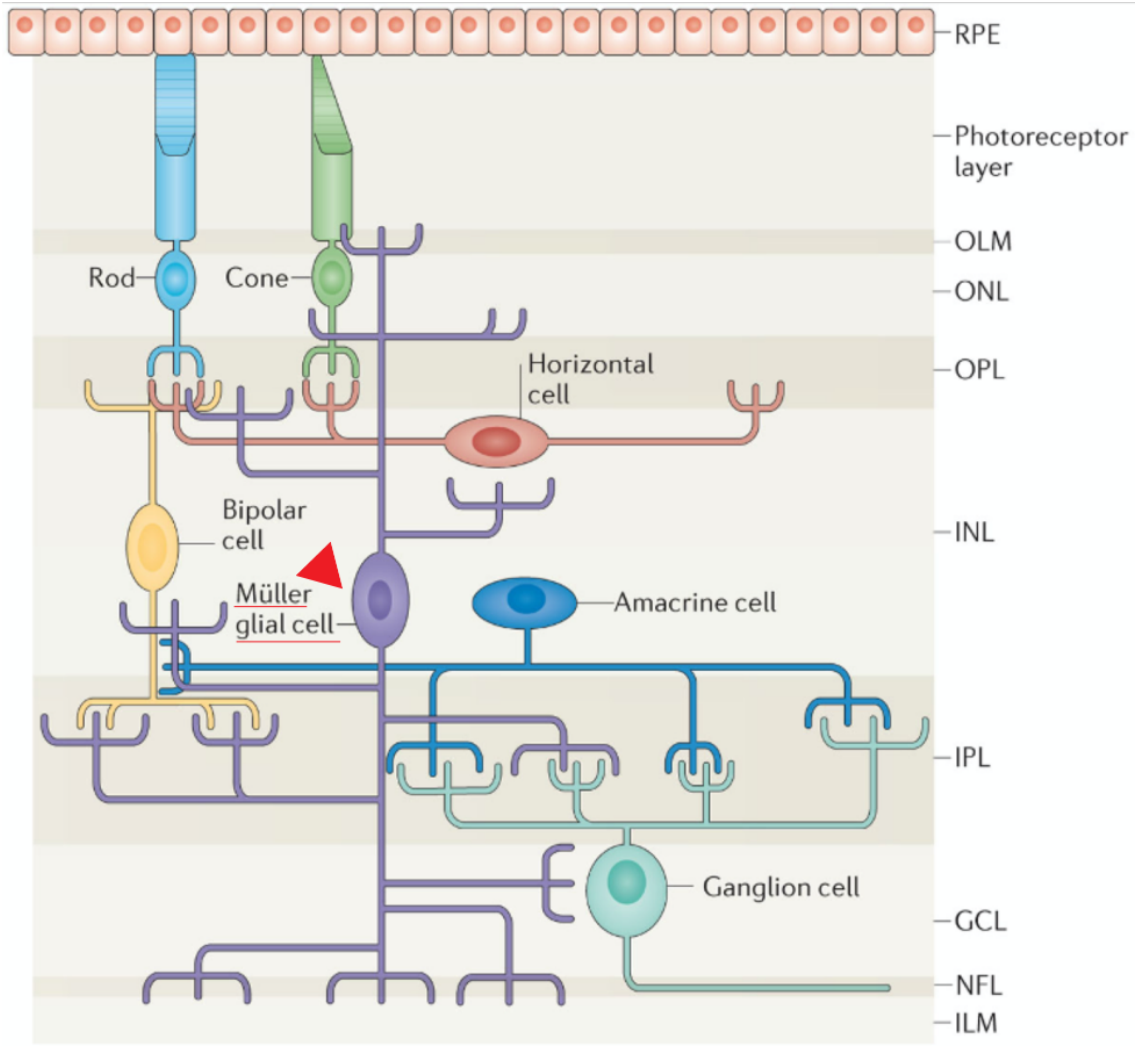

Figure 1: Retinal Neurons and Müller Glial Cell.

A modified schematic to illustrates the structure of the vertebrate retina from Goldman's review [104]. The soma of the six types of primary retinal neurons and Müller glial cell (purple) are organized into three lamina layers and two synaptic layers in a mature retina. The outer nuclear layer (ONL) consists of the cell bodies of rod and cone photoreceptors. The inner nuclear layer (INL) contains the cell bodies of interneurons horizontal, bipolar, and amacrine cells, along with Müller glia. The projection neurons—the retinal ganglion cells, are located in the ganglion cell layer (GCL) with their axons extending beneath the GCL and forming a nerve fiber layer (NFL). The outer plexiform layer (OPL) houses synapses between photoreceptors and interneurons. Dendritic processes of the interneurons and retinal ganglion cells form synaptic connections in the inner plexiform layer (IPL). Müller glia processes span the entire retina with their end-feet forming the outer limiting membrane (OLM) and the inner limiting membrane (ILM). In addition, the retinal pigment epithelium (RPE) cells have their microvilli surrounding the tips of the photoreceptors' outer segment in the sub-retinal space.

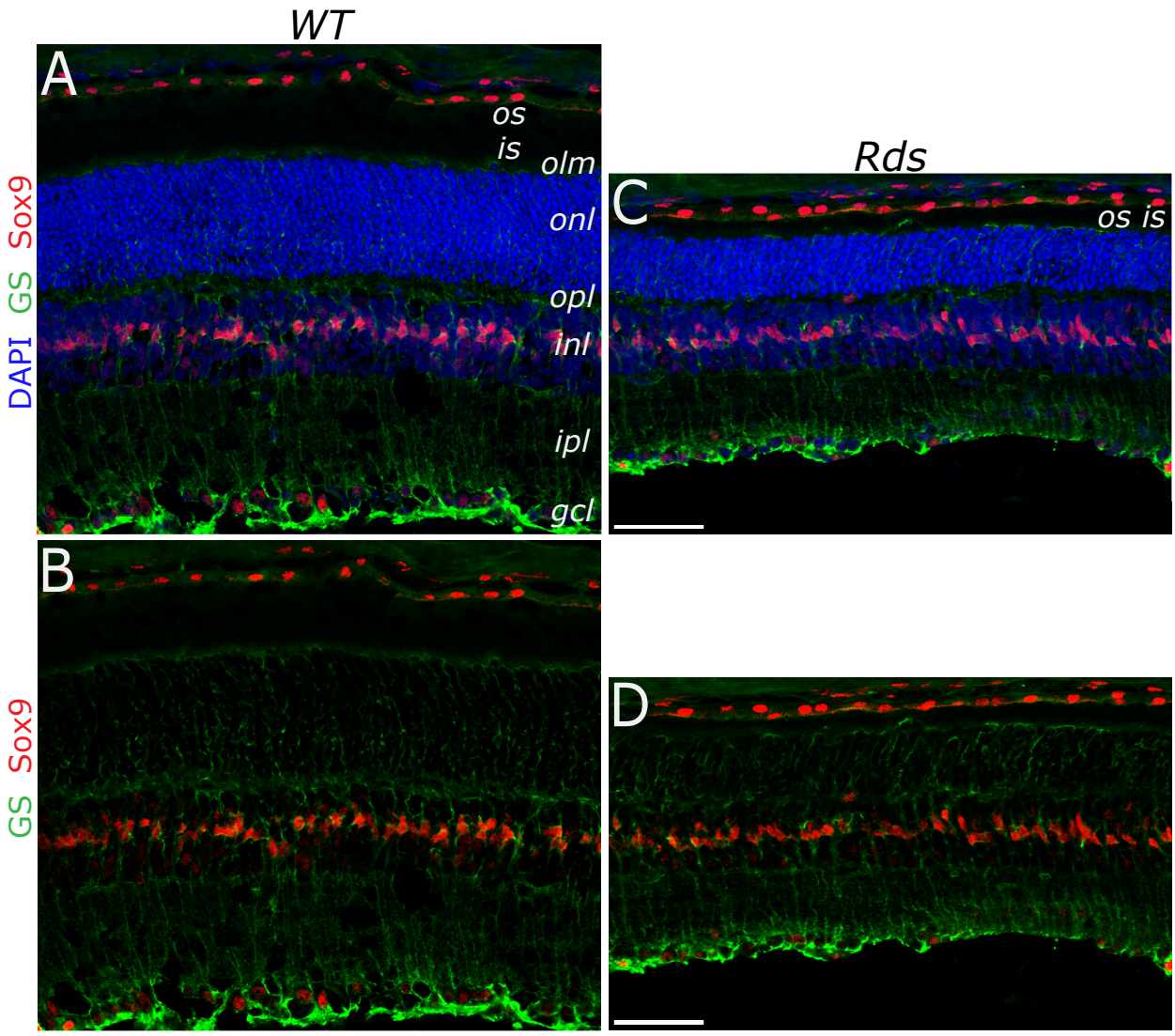

Figure 2: Müller Glial Cells in Wild Type and Degenerating *Rds* Retina.

Confocal images of P33 *WT* **(A, B)** and *Rds* **(C, D)** retinas immunostained for Sox9 (red) and glutamine synthetase (GS, green), which are two markers labeled Müller nuclei and processes, respectively. DAPI staining (blue) **(A, C)** shows thinning of the ONL in the *Rds* retina compared with the *WT* retina, reflecting photoreceptor degeneration at P33.

os—outer segment; *is*—inner segment; *olm*—outer limiting membrane; *onl*—outer nuclear layer; *opl*—outer plexiform layer; *inl*—inner nuclear layer; *ipl*—inner plexiform layer; *gcl*—ganglion cell layer.

[Scale bars: (A–D) 50 μm]

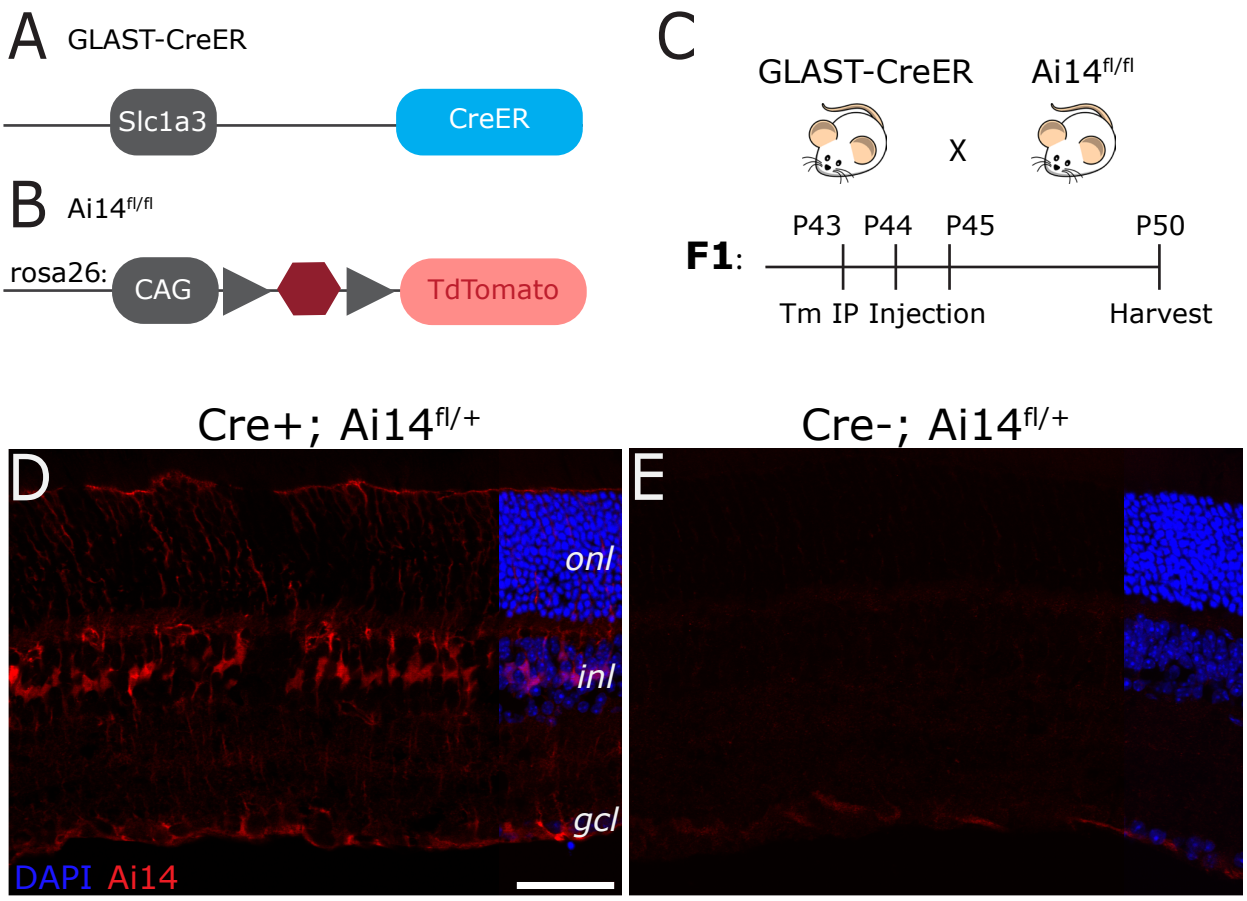

Figure 3: Genetic Labeling of Müller Glia with Inducible CreER and Reporter.

(A) The *GLAST-CreER* transgenic mouse encodes the glial specific Slc1a3 promoter followed by the inducible CreER recombinase.
(B) The *Ai14$^{fl/fl}$* mouse line encodes the CAG promoter upstream of a loxP site-flanked STOP cassette followed by tdTomato reporter at the rosa26 locus.
(C) The genetic cross to produce F1 and experimental timeline to test the specificity of *GLAST-CreER* using tamoxifen (Tm).
(D–E) Confocal images of P50 retinal cross-sections co-stained with DAPI (blue) showed specific labeling of Müller glia with tdTomato reporter (red) in the Cre+ retina compared with the Cre- retina.

onl—outer nuclear layer; *inl*—inner nuclear layer; *gcl*—ganglion cell layer.

[Scale bars: (D–E) 50 μm]

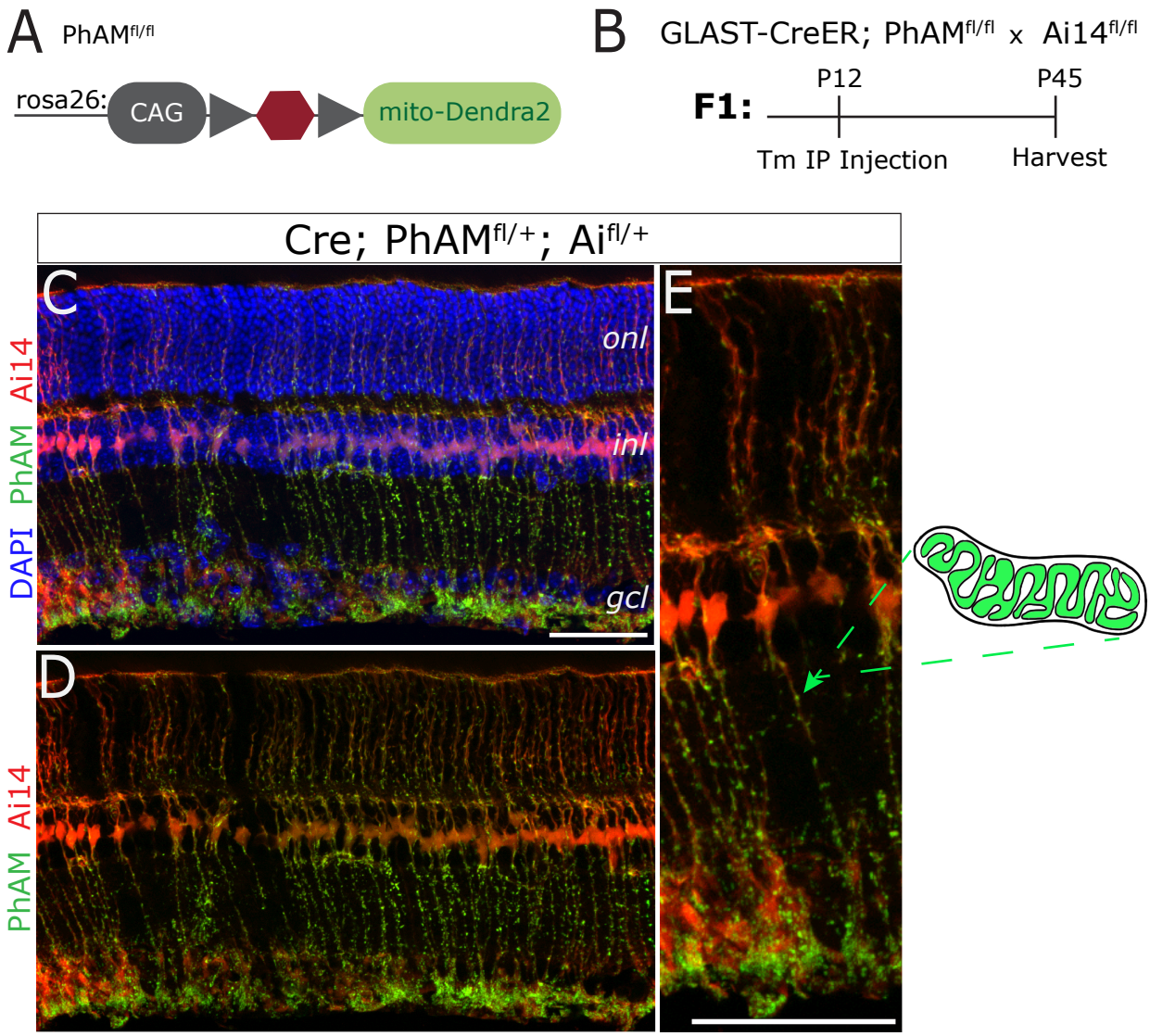

Figure 4: Genetic Labeling of Müller Glial Mitochondria with *PhAM* Reporter.

(A) Schematic of *PhAM*$^{fl/fl}$ transgene at rosa26 locus encoding the CAG promoter upstream of a loxP site-flanked STOP cassette followed by a mitochondrial targeting Dendra2 fluorescence reporter.
(B) Genetic cross using *GLAST-CreER* and *PhAM*$^{fl/fl}$ to produce F1 and the experimental timeline to induce both *Ai* and *PhAM* reporters to label Müller glial cells and their mitochondria.
(C–D) Confocal images of retinal cross-section showed specific labeling of Müller glia with tdTomato (red) and mitochondria with *PhAM* (green) (10 µm Z-stack with C showing DAPI labeling).
(E) An expanded image shows mito-Dendra2 targeting the mitochondrial matrix of Müller glia. Arrow points to a single Müller glial mitochondrion.

onl—outer nuclear layer; *inl*—inner nuclear layer; *gcl*—ganglion cell layer.
[Scale bars: (C–E) 50 µm]

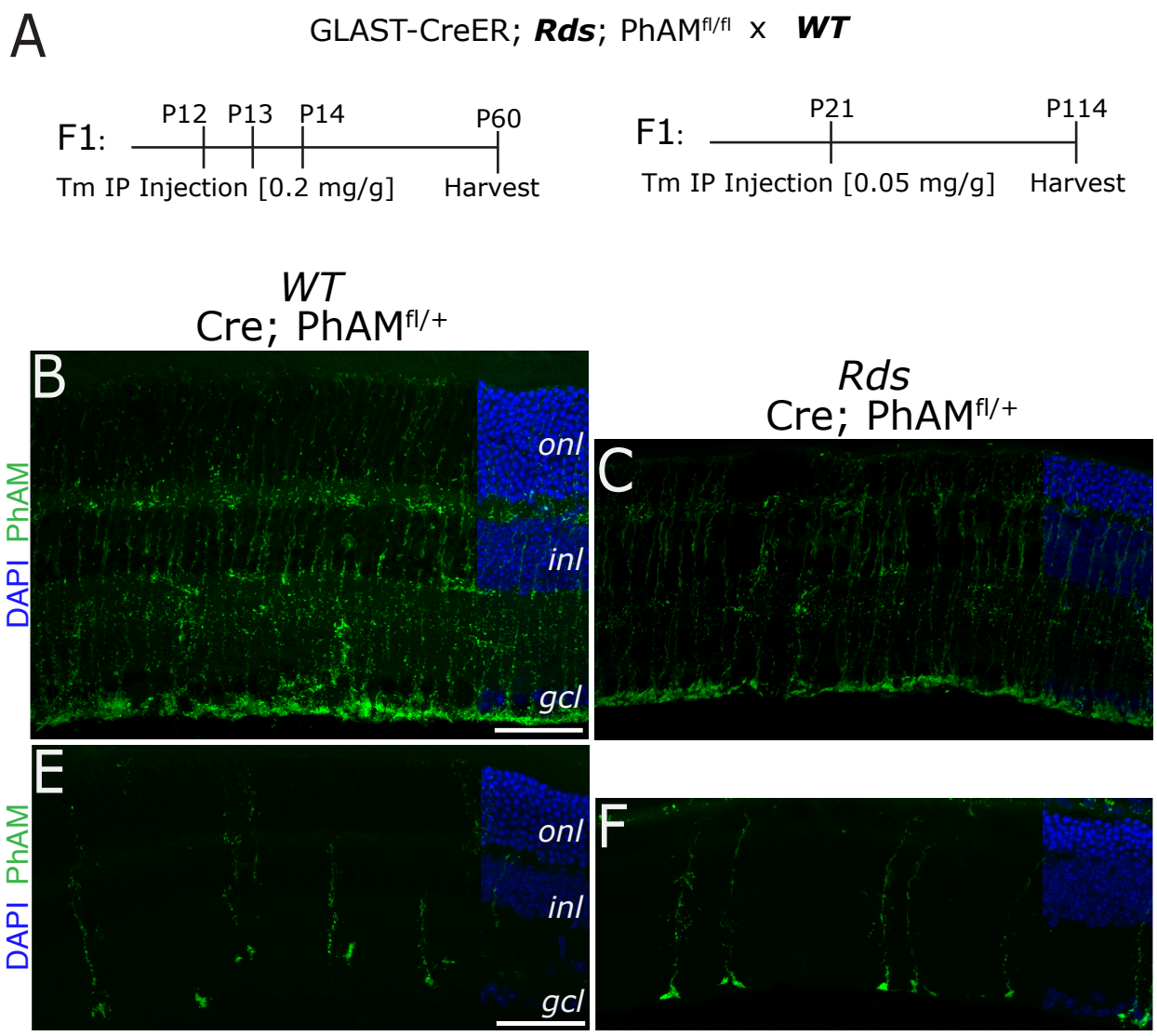

Figure 5: Densely and Sparsely Labeled Müller Glia Mitochondria.

(A) Genetic cross **(top)** and experimental timelines to produce densely labeled **(left)** and sparsely labeled **(right)** Müller mitochondria with *PhAM* reporter, respectively.
(B–C) 10 µm Z-stack confocal images of retinal cross-section show densely labeled Müller glia mitochondria in *WT* **(B)** and *Rds* **(C)** at P60.
(E–F) 25 µm Z-stack confocal images of retinal cross-section capture mitochondria in sparsely labeled single Müller glial cells in *WT* **(E)** and *Rds* **(F)** at P114.

onl—outer nuclear layer; *inl*—inner nuclear layer; *gcl*—ganglion cell layer.

[Scale bars: (B–C, E–F) 50 µm]

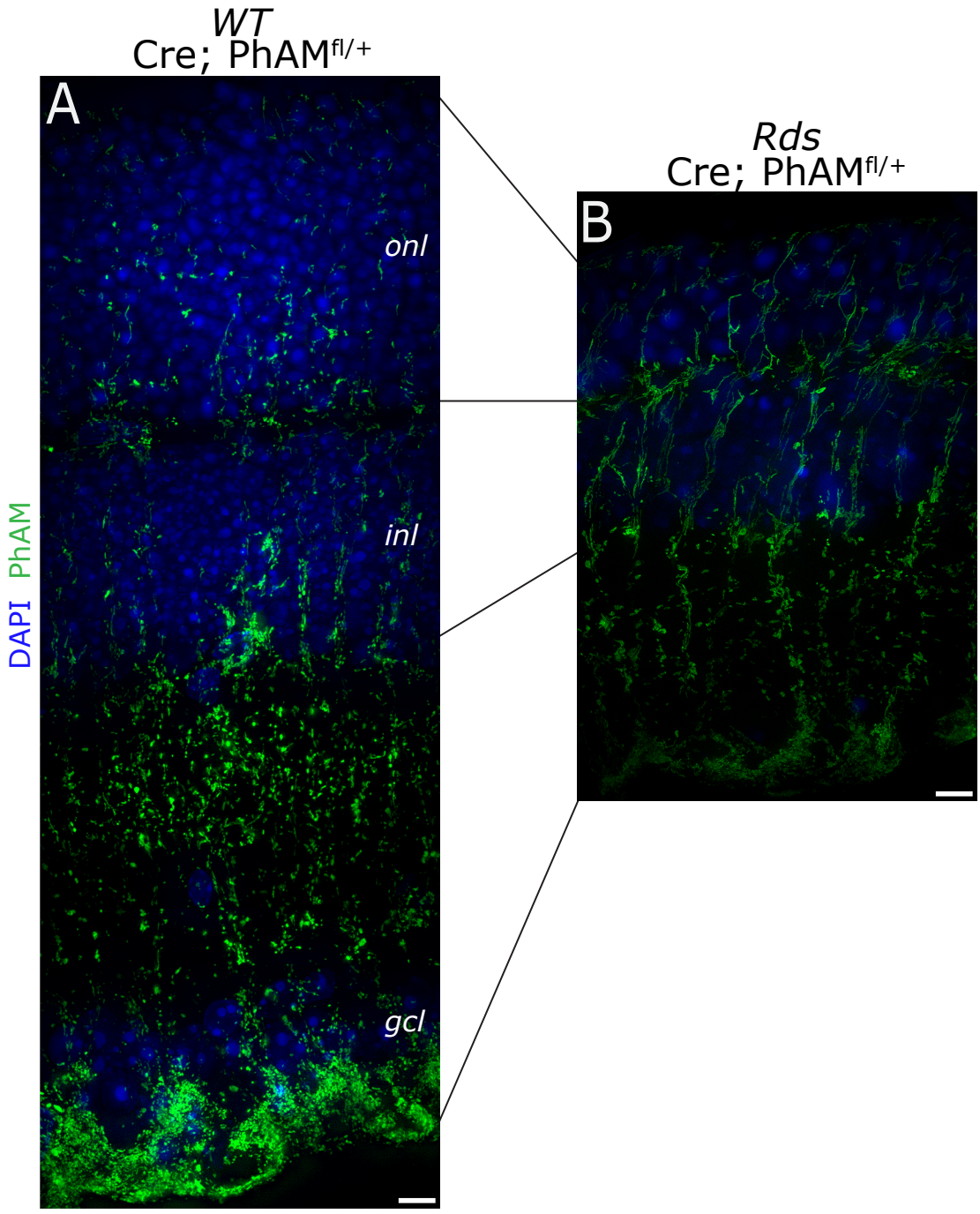

Figure 6: Structured Illumination Microscopy Applied to Reveal the Morphology of Müller Glial Mitochondria

Super-resolution SIM images of retinal cross-sections capture Müller mitochondrial morphology. (**A**) P60 *WT* retina (20 µm Z-stack reconstructed) and (**B**) *Rds* retina (15 µm Z-stack reconstructed).

onl—outer nuclear layer; *inl*—inner nuclear layer; *gcl*—ganglion cell layer. [Scale bars: (A–B) 5 µm]

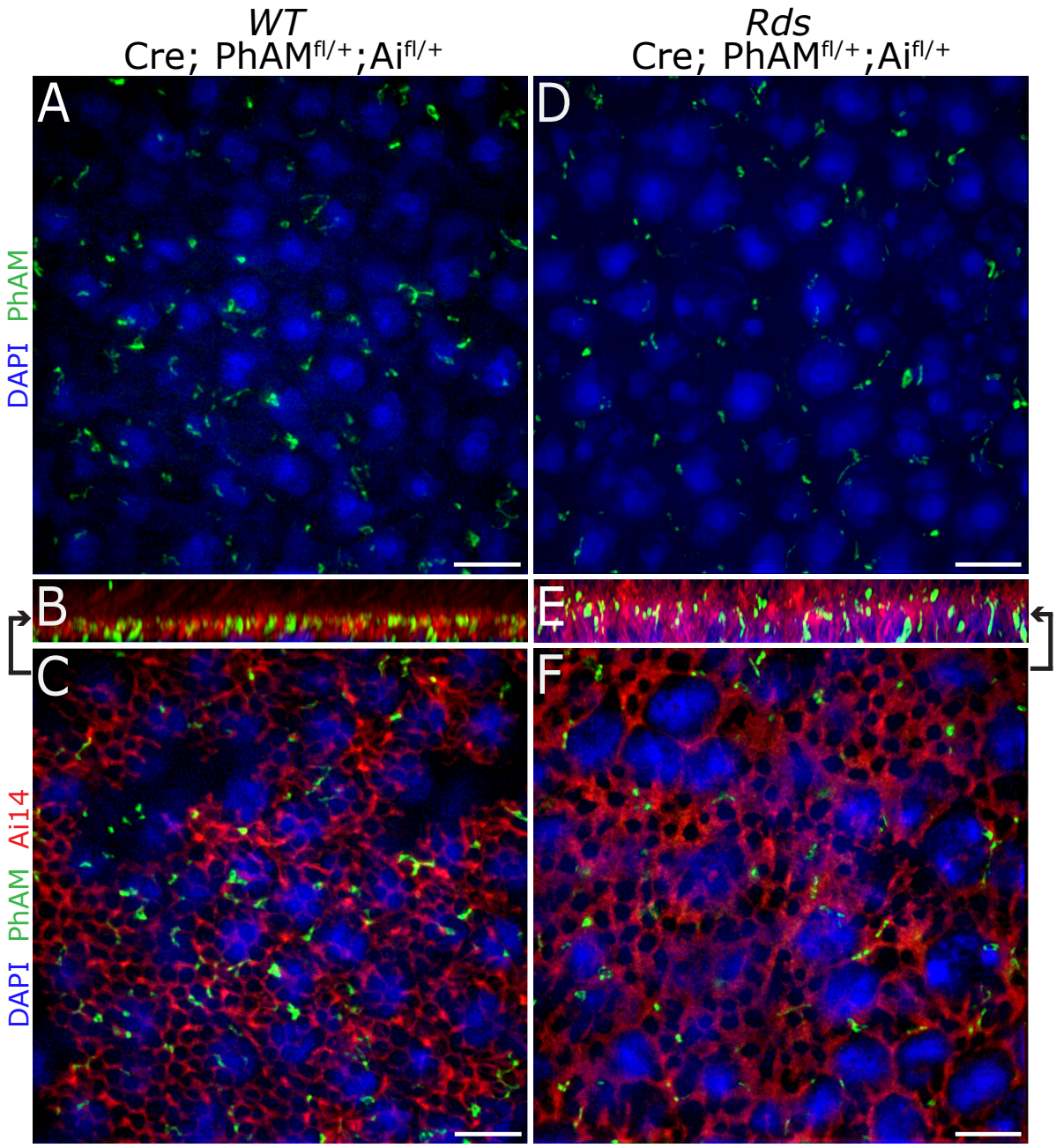

Figure 7: Müller Glial Mitochondria at the Outer Limiting Membrane.

(A, D) En face view of reconstructed SIM images of *PhAM* reporter (5 µm Z-stack) of flat-mounted P64 *WT* **(A)** and P61 *Rds* **(D)** retinas co-labeled with DAPI (blue) for onl nuclei, capturing Müller glial mitochondria at the outer limiting membrane.
(B, E) Volume side view of *PhAM* reporter (5 µm Z-stack) merged with Müller processes labeled with *Ai14* reporter (red). Note the abnormal sprouting of the *Rds* Müller processes.
(C, F) En face view of merged SIM images (1 µm) at the position pointed by arrows from panels **(B)** and **(E)**.
[Scale bars: (A–F) 5 µm]

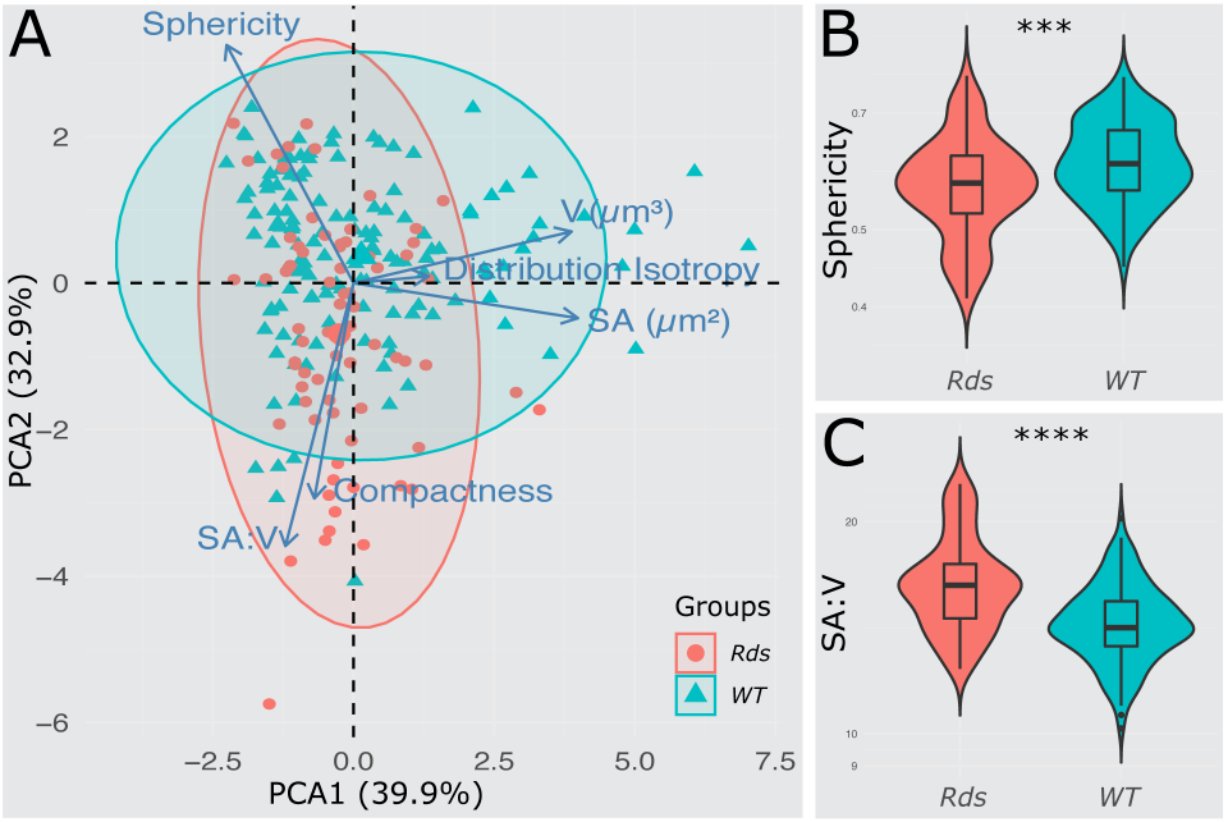

Figure 8: Quantitative Analysis of Müller Mitochondrial Morphology at the Outer Limiting Membrane.

(A) The principal component analysis (PCA) separates Müller mitochondrial geometry of P64 *WT* and P61 *Rds* retina. Separation in PCA1 is mainly driven by surface area and volume, while SA:V, compactness, and sphericity contribute to separation in PCA2.
(B, C) Violin and box plots show significant sphericity (B) and surface area versus volume (C) differences between *WT* and *Rds*.

n = 4 (40x40 µm region in XY of SIM 5 µm Z-stacks) from 1 animal for *WT*. n = 4 from 2 animals for *Rds*.
[*** $p < 0.001$, **** $p < 0.0001$]

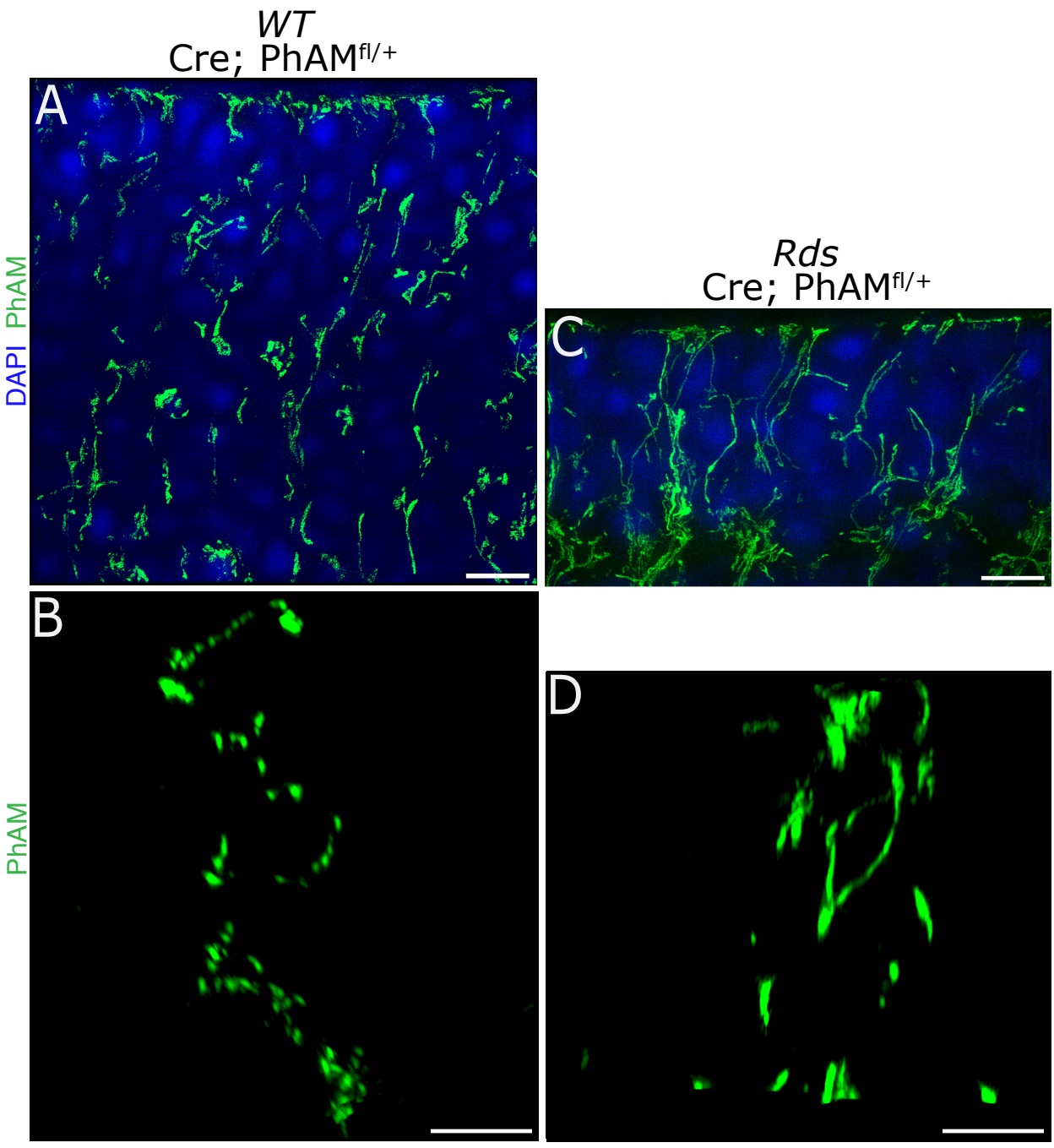

Figure 9: Müller Glial Mitochondria in the Outer Nuclear Layer.

(A, C) Z-stack reconstructed SIM images of *WT* (15 µm) and *Rds* (18 µm) retinal cross-section show Müller glia mitochondria at P60 in the outer nuclear layer. **(B, D)** Volume view of mitochondria of a single Müller cell of P114 whole-mount retinas at the outer nuclear layer.

[Scale bars: (A–D) 5 um]

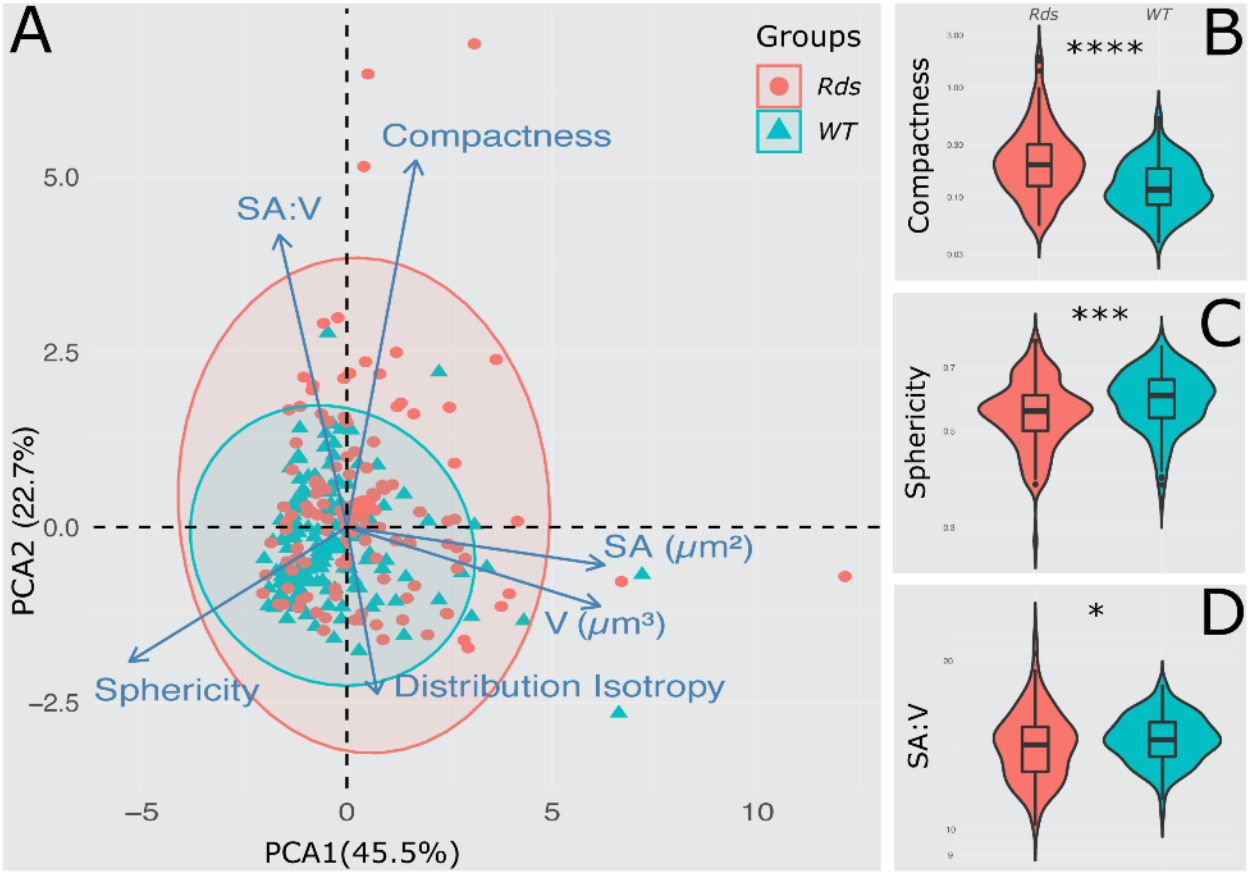

Figure 10: Quantitative Analysis of Müller Mitochondrial Morphology in the Outer Nuclear Layer.

(A) The PCA separates Müller mitochondrial geometry of *WT* and *Rds* retina at P114. PCA1 contribution: surface area, volume, and sphericity; PCA2 contribution: compactness and SA:V.
(B, C, D) Violin and box plots show significant geometrical differences between the two populations of Müller mitochondria.

n = 8 individual Müller glia for each genotype.
[**** $p < 0.0001$, *** $p < 0.001$, * $p < 0.05$]

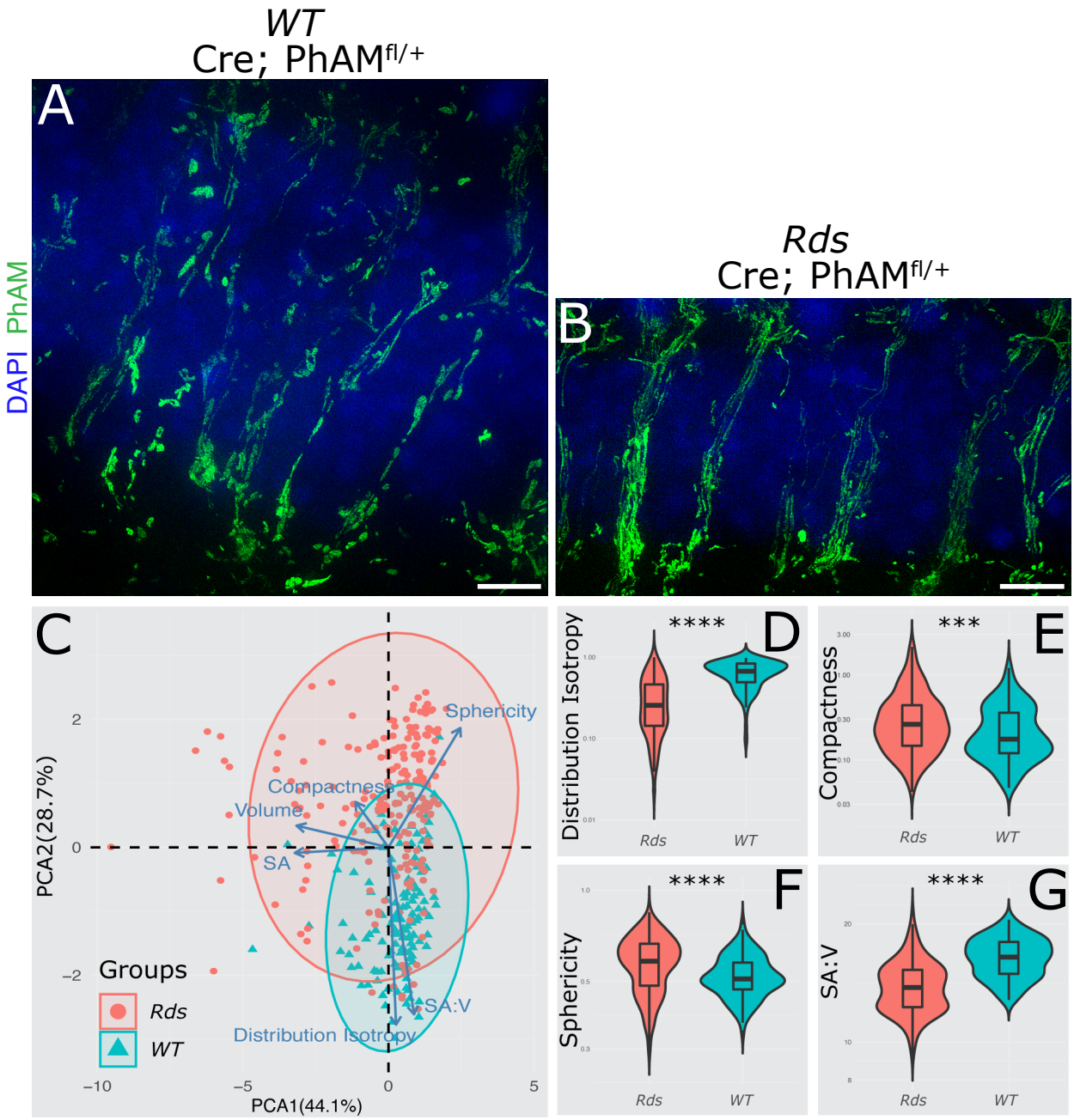

Figure 11: Müller Mitochondrial Morphology at the Inner Nuclear Layer.

(A, B) 18 µm Z-stack reconstructed SIM images of *WT* and *Rds* retinal cross-sections at P60 show merged *PhAM* and DAPI labeling at the inner nuclear layer.
(C) The principal component analysis separates Müller glial mitochondrial geometry of *WT* and *Rds* retinas at P114. PCA1 contribution: surface area, volume, and sphericity; PCA2 contribution: distribution isotropy and SA:V.
(D–G) Violin and box plots show significant geometrical differences between the *WT* and *Rds* Müller mitochondria.
n = 8 individual Müller glia for *WT*, and n = 12 individual Müller glia for *Rds* [**** $p < 0.0001$, * $p < 0.05$]

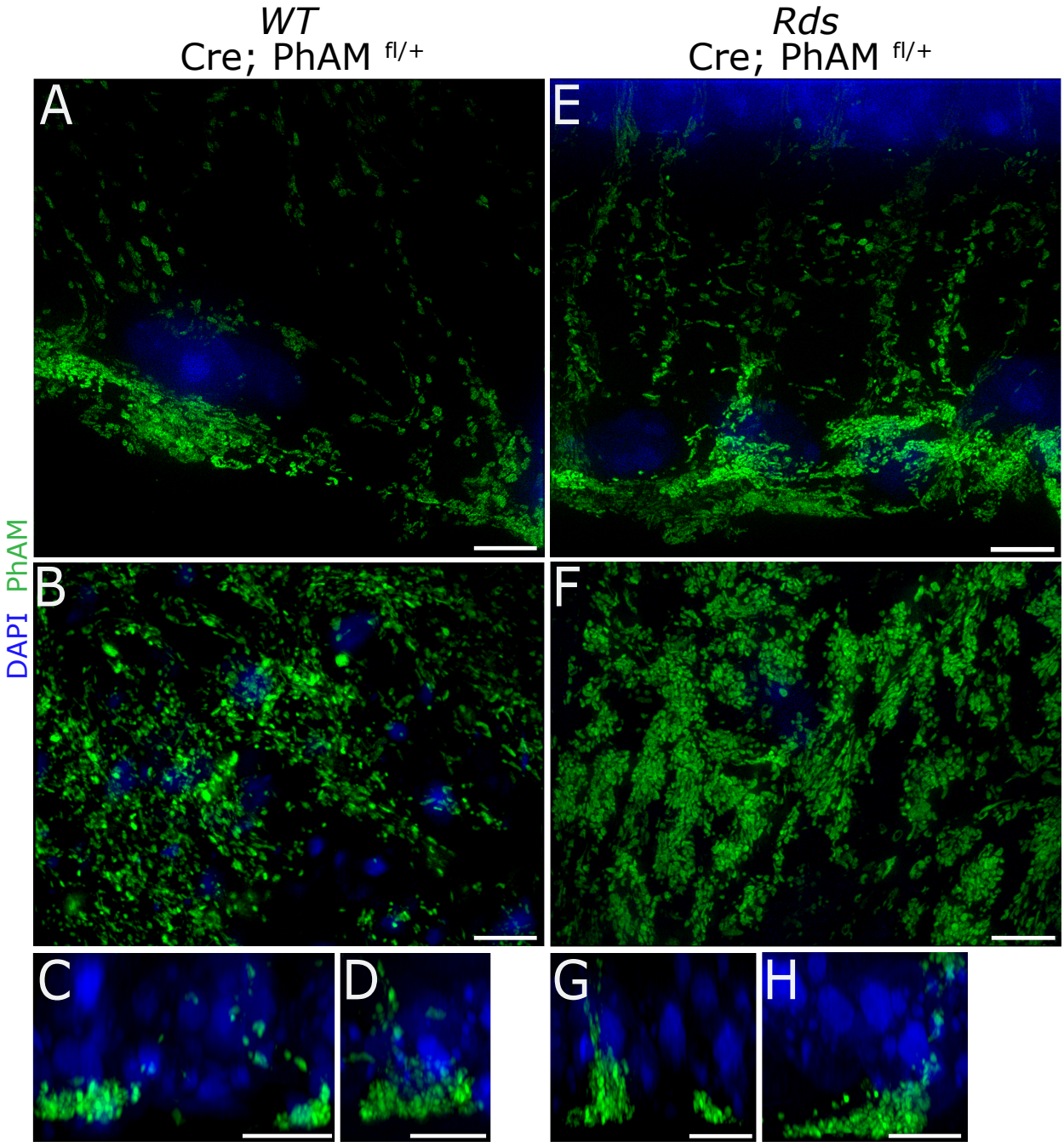

Figure 12: Müller Glial Mitochondria at the Ganglion Cell Layer.

(A, E) Z-stack reconstruction SIM images of P60 *WT* (15 µm) and *Rds* (18 µm) retinal cross-section at the ganglion cell layer.
(B, F) 1 µm Z-stack images of flat-mounted retinas showed mitochondria (green) of Müller glial cells at the end feet.
(C, D, G, H) Volume view of reconstructed mitochondria from single Müller end-feet of flat-mounted retinas at P114 for *WT* **(C, D)** and *Rds* **(G, H)**.
[Scale bars: (A–H) 5 um]

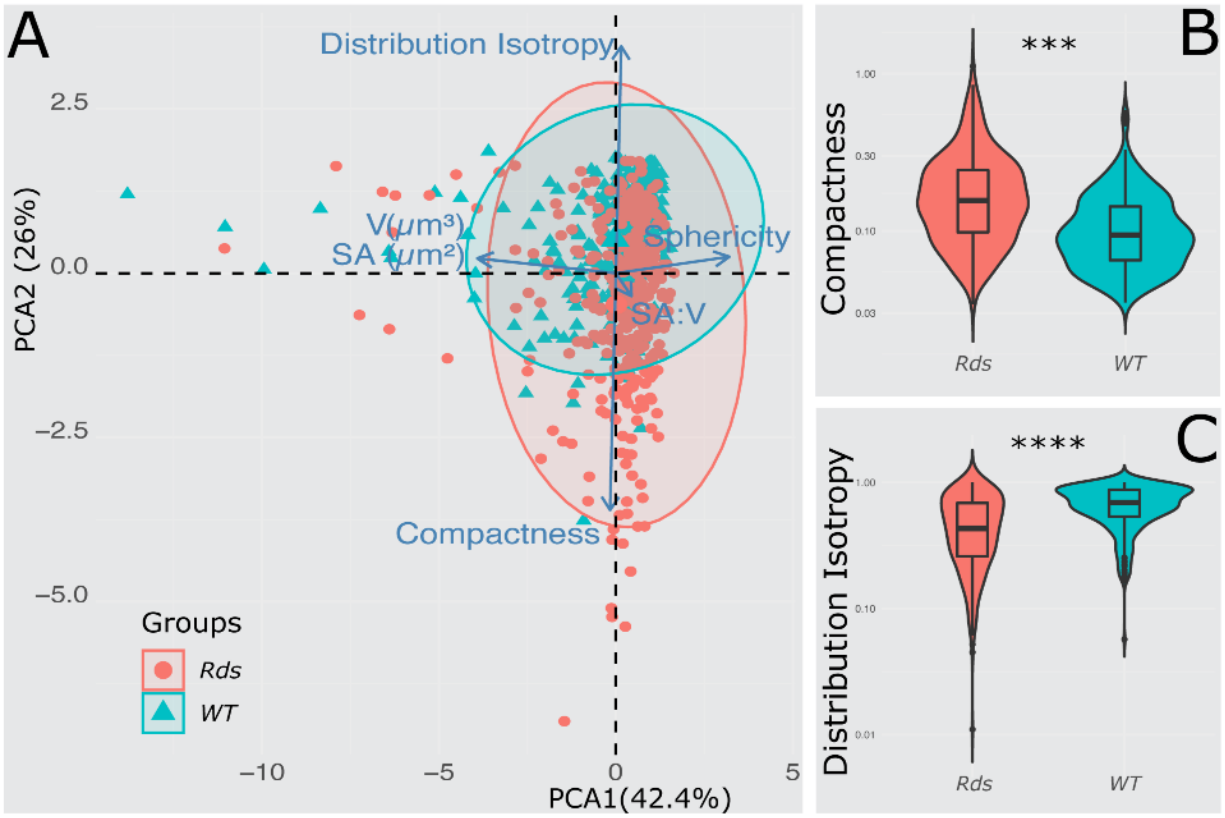

Figure 13: Quantitative Analysis of Müller Mitochondrial Morphology at the Ganglion Cell Layer.

(A) The principal component analysis separates Müller glial mitochondrial geometry of *WT* and *Rds* retinas at P114. Separation in PCA1 is mainly driven by surface area, volume, and sphericity, while SA:V, compactness, and distribution isotropy contribute to separation in PCA2.
(B, C) Violin and box plots indicate significant geometrical differences between the *WT* and *Rds* Müller mitochondria.

n = 11 individual Müller glia for *WT,* and n = 9 individual Müller glia for *Rds*
[*** p < 0.001, *** p <0.0001]

Table 1: Summary of Antibodies.

	Antibody	Manufacturer (Catalog#)	Type	Host	Dilution
Primary Antibodies					
	Sox9	Millipore-Sigma (5535)	Polyclonal	Mouse	1:400
	Glutamine synthetase (GS)	Millipore-Sigma (MAB302)	Monoclonal	Rabbit	1:50
Secondary Antibodies					
	Alexa 488 (Anti-Mouse)	Invitrogen (A-21202)	Polyclonal	Donkey	1:500
	Alexa 594 (Anti-Rabbit)	Invitrogen (A-21207)	Polyclonal	Donkey	1:500

Table 2: Descriptions of Mitochondrial Morphology Parameters.

Feature	Description	Reference
Compactness	Variance of radial distance/volume	[72]
Distribution isotropy	The sum of ratios of the second moments in each combination of orientations	
Sphericity	The ratio of the surface area of a sphere with the same volume as the object to the surface area of the object	
SA:V	Surface to volume ratio	

Table 3-A: Statistic for Independent Samples T-Test Comparing Müller Mitochondria Morphology at the Outer Limiting Membrane.

	W	p
Volume (μm³)	5939.000	0.019
Surface Area (μm²)	4959.000	0.991
Compactness	4185.000	0.062
Distribution Isotropy	4420.000	0.192
Sphericity	6355.500	< .001
SA:V	2651.500	< .001

Note. Mann-Whitney U test.

Table 3-B: Descriptive Values for Müller Mitochondria Morphology at the Outer Limiting Membrane.

	Group	Mean	SD	SE
Volume (μm³)	*WT*	0.192	0.098	0.008
	rds	0.153	0.045	0.005
Surface Area (μm²)	*WT*	2.664	1.107	0.095
	rds	2.465	0.658	0.077
Compactness	*WT*	0.164	0.115	0.010
	rds	0.219	0.184	0.022
Distribution Isotropy	*WT*	0.581	0.227	0.019
	rds	0.623	0.229	0.027
Sphericity	*WT*	0.610	0.072	0.006
	rds	0.570	0.081	0.009
SA:V	*WT*	14.418	1.837	0.158
	rds	16.396	2.550	0.298

Table 4-A: Statistic for Independent Samples T-Test Comparing Müller Mitochondria Morphology at the Outer Nuclear Layer.

	W	p
Volume (μm³)	6444.000	< .001
Surface Area (μm²)	6350.500	< .001
Compactness	5387.000	< .001
Distribution Isotropy	12782.500	< .001
Sphericity	11848.000	< .001
SA:V	10678.500	0.049

Note. Mann-Whitney U test.

Table 4-B: Descriptive Values for Müller Mitochondria Morphology at the Outer Nuclear Layer.

	Group	Mean	SD	SE
Volume (μm³)	*WT*	0.218	0.186	0.015
	rds	0.305	0.256	0.023
Surface Area (μm²)	*WT*	3.058	2.245	0.184
	rds	4.148	3.223	0.287
Compactness	*WT*	0.143	0.085	0.007
	rds	0.279	0.284	0.025
Distribution Isotropy	*WT*	0.649	0.194	0.016
	rds	0.498	0.254	0.023
Sphericity	*WT*	0.596	0.089	0.007
	rds	0.555	0.097	0.009
SA:V	*WT*	14.557	1.415	0.116
	rds	14.241	2.068	0.184

Table 5-A: Statistic for Independent Samples T-Test Comparing Müller Mitochondria Morphology at the Inner Nuclear Layer.

	W	p
Volume (μm³)	11528.500	0.015
Surface Area (μm²)	13992.000	0.732
Compactness	10818.500	0.001
Distribution Isotropy	23105.500	< .001
Sphericity	9538.500	< .001
SA:V	22319.000	< .001

Note. Mann-Whitney U test.

Table 5-B: Descriptive Values for Müller Mitochondria Morphology at the Inner Nuclear Layer.

	Group	Mean	SD	SE
Volume (μm³)	*WT*	0.215	0.148	0.013
	rds	0.330	0.330	0.022
Surface Area (μm²)	*WT*	3.432	2.032	0.182
	rds	4.300	3.901	0.264
Compactness	*WT*	0.259	0.211	0.019
	rds	0.367	0.349	0.024
Distribution Isotropy	*WT*	0.647	0.216	0.019
	rds	0.318	0.229	0.016
Sphericity	*WT*	0.523	0.083	0.007
	rds	0.578	0.115	0.008
SA:V	*WT*	16.443	1.891	0.169
	rds	13.892	2.111	0.143

Table 6-A: Statistic for Independent Samples T-Test Comparing Müller Mitochondria Morphology at the Ganglion Cell Layer.

	W	p
Volume (μm³)	52699.000	0.909
Surface Area (μm²)	52901.500	0.842
Compactness	29861.000	< .001
Distribution Isotropy	74901.000	< .001
Sphericity	51899.500	0.825
SA:V	52470.000	0.986

Note. Mann-Whitney U test.

Table 6-B: Descriptive Values for Müller Mitochondria Morphology at the Ganglion Cell Layer.

	Group	Mean	SD	SE
Volume (μm³)	*WT*	0.423	0.781	0.044
	rds	0.397	0.676	0.037
Surface Area (μm²)	*WT*	6.158	11.080	0.626
	rds	5.654	8.854	0.484
Compactness	*WT*	0.113	0.073	0.004
	rds	0.194	0.145	0.008
Distribution Isotropy	*WT*	0.676	0.222	0.013
	rds	0.478	0.263	0.014
Sphericity	*WT*	0.528	0.123	0.007
	rds	0.534	0.125	0.007
SA:V	*WT*	15.102	1.735	0.098
	rds	15.042	1.926	0.105

REFERENCECS

1. Dowling, J.E., *The retina : an approachable part of the brain*. Rev. ed. 2012, Cambridge, Mass.: Belknap Press of Harvard University Press. xvi, 355 p.
2. Vecino, E., et al., *Glia-neuron interactions in the mammalian retina.* Prog Retin Eye Res, 2016. **51**: p. 1-40.
3. Turner, D.L. and C.L. Cepko, *A common progenitor for neurons and glia persists in rat retina late in development.* Nature, 1987. **328**(6126): p. 131-6.
4. Rapaport, D.H., et al., *Timing and topography of cell genesis in the rat retina.* J Comp Neurol, 2004. **474**(2): p. 304-24.
5. Dowling, J.E., *The retina : an approachable part of the brain*. 1987, Cambridge, Mass.: Belknap Press of Harvard University Press. xii, 282 p., 4 p. of plates.
6. Hoon, M., et al., *Functional architecture of the retina: development and disease.* Prog Retin Eye Res, 2014. **42**: p. 44-84.
7. Amini, R., M. Rocha-Martins, and C. Norden, *Neuronal Migration and Lamination in the Vertebrate Retina.* Front Neurosci, 2017. **11**: p. 742.
8. MacDonald, R.B., et al., *Muller glia provide essential tensile strength to the developing retina.* J Cell Biol, 2015. **210**(7): p. 1075-83.
9. Wang, J., et al., *Anatomy and spatial organization of Muller glia in mouse retina.* J Comp Neurol, 2017. **525**(8): p. 1759-1777.
10. Derouiche, A., et al., *Beyond polarity: functional membrane domains in astrocytes and Muller cells.* Neurochem Res, 2012. **37**(11): p. 2513-23.

11. Kolb, H., *Glial Cells of the Retina*, in *Webvision: The Organization of the Retina and Visual System*, H. Kolb, E. Fernandez, and R. Nelson, Editors. 1995: Salt Lake City (UT).

12. Wang, Y.P., et al., *Development of normal retinal organization depends on Sonic hedgehog signaling from ganglion cells.* Nat Neurosci, 2002. **5**(9): p. 831-2.

13. Dubois-Dauphin, M., et al., *Early postnatal Muller cell death leads to retinal but not optic nerve degeneration in NSE-Hu-Bcl-2 transgenic mice.* Neuroscience, 2000. **95**(1): p. 9-21.

14. Jadhav, A.P., K. Roesch, and C.L. Cepko, *Development and neurogenic potential of Muller glial cells in the vertebrate retina.* Prog Retin Eye Res, 2009. **28**(4): p. 249-62.

15. Fischer, A.J. and T.A. Reh, *Muller glia are a potential source of neural regeneration in the postnatal chicken retina.* Nat Neurosci, 2001. **4**(3): p. 247-52.

16. Bernardos, R.L., et al., *Late-stage neuronal progenitors in the retina are radial Muller glia that function as retinal stem cells.* J Neurosci, 2007. **27**(26): p. 7028-40.

17. Fausett, B.V. and D. Goldman, *A role for alpha1 tubulin-expressing Muller glia in regeneration of the injured zebrafish retina.* J Neurosci, 2006. **26**(23): p. 6303-13.

18. Hamon, A., et al., *Linking YAP to Muller Glia Quiescence Exit in the Degenerative Retina.* Cell Rep, 2019. **27**(6): p. 1712-1725 e6.

19. Hamon, A., et al., *Muller glial cell-dependent regeneration of the neural retina: An overview across vertebrate model systems.* Dev Dyn, 2016. **245**(7): p. 727-38.

20. Yao, K., et al., *Restoration of vision after de novo genesis of rod photoreceptors in mammalian retinas.* Nature, 2018. **560**(7719): p. 484-488.

21. Conner, C., et al., *Repressing notch signaling and expressing TNFalpha are sufficient to mimic retinal regeneration by inducing Muller glial proliferation to generate committed progenitor cells.* J Neurosci, 2014. **34**(43): p. 14403-19.

22. Jorstad, N.L., et al., *Stimulation of functional neuronal regeneration from Muller glia in adult mice.* Nature, 2017. **548**(7665): p. 103-107.

23. Das, S.R., et al., *Muller cells of chicken retina synthesize 11-cis-retinol.* Biochem J, 1992. **285 (Pt 3)**: p. 907-13.

24. Mata, N.L., et al., *Isomerization and oxidation of vitamin a in cone-dominant retinas: a novel pathway for visual-pigment regeneration in daylight.* Neuron, 2002. **36**(1): p. 69-80.

25. Newman, E. and A. Reichenbach, *The Muller cell: a functional element of the retina.* Trends Neurosci, 1996. **19**(8): p. 307-12.

26. Thoreson, W.B. and P. Witkovsky, *Glutamate receptors and circuits in the vertebrate retina.* Prog Retin Eye Res, 1999. **18**(6): p. 765-810.

27. Derouiche, A. and T. Rauen, *Coincidence of L-glutamate/L-aspartate transporter (GLAST) and glutamine synthetase (GS) immunoreactions in*

retinal glia: evidence for coupling of GLAST and GS in transmitter clearance. J Neurosci Res, 1995. **42**(1): p. 131-43.

28. Rauen, T., et al., *High-affinity glutamate transporters in the rat retina: a major role of the glial glutamate transporter GLAST-1 in transmitter clearance.* Cell Tissue Res, 1998. **291**(1): p. 19-31.
29. Toft-Kehler, A.K., et al., *Mitochondrial function in Muller cells - Does it matter?* Mitochondrion, 2017. **36**: p. 43-51.
30. Rauen, T. and M. Wiessner, *Fine tuning of glutamate uptake and degradation in glial cells: common transcriptional regulation of GLAST1 and GS.* Neurochem Int, 2000. **37**(2-3): p. 179-89.
31. Toft-Kehler, A.K., D.M. Skytt, and M. Kolko, *A Perspective on the Muller Cell-Neuron Metabolic Partnership in the Inner Retina.* Mol Neurobiol, 2018. **55**(6): p. 5353-5361.
32. Tsacopoulos, M., J.A. Coles, and G. Van de Werve, *The supply of metabolic substrate from glia to photoreceptors in the retina of the honeybee drone.* J Physiol (Paris), 1987. **82**(4): p. 279-87.
33. Poitry-Yamate, C.L., S. Poitry, and M. Tsacopoulos, *Lactate released by Muller glial cells is metabolized by photoreceptors from mammalian retina.* J Neurosci, 1995. **15**(7 Pt 2): p. 5179-91.
34. Winkler, B.S., et al., *Energy metabolism in human retinal Muller cells.* Invest Ophthalmol Vis Sci, 2000. **41**(10): p. 3183-90.
35. Lindsay, K.J., et al., *Pyruvate kinase and aspartate-glutamate carrier distributions reveal key metabolic links between neurons and glia in retina.* Proc Natl Acad Sci U S A, 2014. **111**(43): p. 15579-84.

36. Kanow, M.A., et al., *Biochemical adaptations of the retina and retinal pigment epithelium support a metabolic ecosystem in the vertebrate eye.* Elife, 2017. **6**.

37. Rueda, E.M., et al., *The cellular and compartmental profile of mouse retinal glycolysis, tricarboxylic acid cycle, oxidative phosphorylation, and ~P transferring kinases.* Mol Vis, 2016. **22**: p. 847-85.

38. Karakucuk, S. and G.E. Mirza, *Ophthalmological effects of high altitude.* Ophthalmic Res, 2000. **32**(1): p. 30-40.

39. Wiedman, M. and G.C. Tabin, *High-altitude retinopathy and altitude illness.* Ophthalmology, 1999. **106**(10): p. 1924-6; discussion 1927.

40. Stenslokken, K.O., et al., *Effect of anoxia on the electroretinogram of three anoxia-tolerant vertebrates.* Comp Biochem Physiol A Mol Integr Physiol, 2008. **150**(4): p. 395-403.

41. Wong-Riley, M.T., *Energy metabolism of the visual system.* Eye Brain, 2010. **2**: p. 99-116.

42. Ferrington, D.A., C.R. Fisher, and R.A. Kowluru, *Mitochondrial Defects Drive Degenerative Retinal Diseases.* Trends Mol Med, 2020. **26**(1): p. 105-118.

43. Parmeggiani, F., *Clinics, epidemiology and genetics of retinitis pigmentosa.* Curr Genomics, 2011. **12**(4): p. 236-7.

44. Hamel, C., *Retinitis pigmentosa.* Orphanet J Rare Dis, 2006. **1**: p. 40.

45. Hartong, D.T., E.L. Berson, and T.P. Dryja, *Retinitis pigmentosa.* Lancet, 2006. **368**(9549): p. 1795-809.

46. Li, Z.Y., D.E. Possin, and A.H. Milam, *Histopathology of bone spicule pigmentation in retinitis pigmentosa.* Ophthalmology, 1995. **102**(5): p. 805-16.

47. Milam, A.H., Z.Y. Li, and R.N. Fariss, *Histopathology of the human retina in retinitis pigmentosa.* Prog Retin Eye Res, 1998. **17**(2): p. 175-205.

48. Daiger, S.P., L.S. Sullivan, and S.J. Bowne, *Genes and mutations causing retinitis pigmentosa.* Clin Genet, 2013. **84**(2): p. 132-41.

49. Roesch, K., M.B. Stadler, and C.L. Cepko, *Gene expression changes within Muller glial cells in retinitis pigmentosa.* Mol Vis, 2012. **18**: p. 1197-214.

50. Punzo, C., K. Kornacker, and C.L. Cepko, *Stimulation of the insulin/mTOR pathway delays cone death in a mouse model of retinitis pigmentosa.* Nat Neurosci, 2009. **12**(1): p. 44-52.

51. Ait-Ali, N., et al., *Rod-derived cone viability factor promotes cone survival by stimulating aerobic glycolysis.* Cell, 2015. **161**(4): p. 817-32.

52. Chinchore, Y., et al., *Glycolytic reliance promotes anabolism in photoreceptors.* Elife, 2017. **6**.

53. Rajala, A., et al., *Pyruvate kinase M2 regulates photoreceptor structure, function, and viability.* Cell Death Dis, 2018. **9**(2): p. 240.

54. Rajala, A., et al., *Pyruvate kinase M2 isoform deletion in cone photoreceptors results in age-related cone degeneration.* Cell Death Dis, 2018. **9**(7): p. 737.

55. Narayan, D.S., et al., *A review of the mechanisms of cone degeneration in retinitis pigmentosa.* Acta Ophthalmol, 2016. **94**(8): p. 748-754.

56. Rhee, K.D., et al., *CNTF-mediated protection of photoreceptors requires initial activation of the cytokine receptor gp130 in Muller glial cells.* Proc Natl Acad Sci U S A, 2013. **110**(47): p. E4520-9.

57. Bringmann, A., et al., *Muller cells in the healthy and diseased retina.* Prog Retin Eye Res, 2006. **25**(4): p. 397-424.

58. Pfeiffer, R.L., et al., *Muller cell metabolic chaos during retinal degeneration.* Exp Eye Res, 2016. **150**: p. 62-70.

59. Chandel, N.S., *Evolution of Mitochondria as Signaling Organelles.* Cell Metab, 2015. **22**(2): p. 204-6.

60. Bock, F.J. and S.W.G. Tait, *Mitochondria as multifaceted regulators of cell death.* Nat Rev Mol Cell Biol, 2020. **21**(2): p. 85-100.

61. Rangaraju, V., et al., *Pleiotropic Mitochondria: The Influence of Mitochondria on Neuronal Development and Disease.* J Neurosci, 2019. **39**(42): p. 8200-8208.

62. Deus, C.M., et al., *Mitochondria-Lysosome Crosstalk: From Physiology to Neurodegeneration.* Trends Mol Med, 2020. **26**(1): p. 71-88.

63. Devine, M.J. and J.T. Kittler, *Mitochondria at the neuronal presynapse in health and disease.* Nat Rev Neurosci, 2018. **19**(2): p. 63-80.

64. Giannoccaro, M.P., et al., *Mitochondrial DNA and primary mitochondrial dysfunction in Parkinson's disease.* Mov Disord, 2017. **32**(3): p. 346-363.

65. Germer, A., et al., *Distribution of mitochondria within Muller cells--I. Correlation with retinal vascularization in different mammalian species.* J Neurocytol, 1998. **27**(5): p. 329-45.

66. Stone, J., et al., *The locations of mitochondria in mammalian photoreceptors: relation to retinal vasculature.* Brain Res, 2008. **1189**: p. 58-69.

67. de Melo, J., et al., *Injury-independent induction of reactive gliosis in retina by loss of function of the LIM homeodomain transcription factor Lhx2.* Proc Natl Acad Sci U S A, 2012. **109**(12): p. 4657-62.

68. Pham, A.H., J.M. McCaffery, and D.C. Chan, *Mouse lines with photo-activatable mitochondria to study mitochondrial dynamics.* Genesis, 2012. **50**(11): p. 833-43.

69. Madisen, L., et al., *A robust and high-throughput Cre reporting and characterization system for the whole mouse brain.* Nat Neurosci, 2010. **13**(1): p. 133-40.

70. Kedzierski, W., et al., *Generation and analysis of transgenic mice expressing P216L-substituted rds/peripherin in rod photoreceptors.* Invest Ophthalmol Vis Sci, 1997. **38**(2): p. 498-509.

71. Schneider, C.A., W.S. Rasband, and K.W. Eliceiri, *NIH Image to ImageJ: 25 years of image analysis.* Nat Methods, 2012. **9**(7): p. 671-5.

72. Vowinckel, J., et al., *MitoLoc: A method for the simultaneous quantification of mitochondrial network morphology and membrane potential in single cells.* Mitochondrion, 2015. **24**: p. 77-86.

73. Linkert, M., et al., *Metadata matters: access to image data in the real world.* J Cell Biol, 2010. **189**(5): p. 777-82.

74. Otsu, N., *A threshold selection method from gray-level histograms.* IEEE Transactions on Systems, Man, and Cybernetics, 1979. **9**(1): p. 62-66.

75. JASP, *JASP (0.13. 1) [Computer software]*. 2020.

76. Sébastien Lê, J.J., François Husson, *An R Package for Multivariable Analysis.* Journal of Statistical Software, 2008. **25**(1): p. 1-18.

77. Hadley, W., *Ggplot2*. 2016, New York, NY: Springer Science+Business Media, LLC. pages cm.

78. West, E.L., et al., *Pharmacological disruption of the outer limiting membrane leads to increased retinal integration of transplanted photoreceptor precursors.* Exp Eye Res, 2008. **86**(4): p. 601-11.

79. den Hollander, A.I., et al., *Mutations in a human homologue of Drosophila crumbs cause retinitis pigmentosa (RP12).* Nat Genet, 1999. **23**(2): p. 217-21.

80. den Hollander, A.I., et al., *Leber congenital amaurosis and retinitis pigmentosa with Coats-like exudative vasculopathy are associated with mutations in the crumbs homologue 1 (CRB1) gene.* Am J Hum Genet, 2001. **69**(1): p. 198-203.

81. Stuck, M.W., S.M. Conley, and M.I. Naash, *Defects in the outer limiting membrane are associated with rosette development in the Nrl-/- retina.* PLoS One, 2012. **7**(3): p. e32484.

82. Iandiev, I., et al., *Atypical gliosis in Muller cells of the slowly degenerating rds mutant mouse retina.* Exp Eye Res, 2006. **82**(3): p. 449-57.

83. Seo, A.Y., et al., *New insights into the role of mitochondria in aging: mitochondrial dynamics and more.* J Cell Sci, 2010. **123**(Pt 15): p. 2533-42.

84. Liesa, M. and O.S. Shirihai, *Mitochondrial dynamics in the regulation of nutrient utilization and energy expenditure.* Cell Metab, 2013. **17**(4): p. 491-506.

85. Pfeiffer, R.L., R.E. Marc, and B.W. Jones, *Muller Cell Metabolic Signatures: Evolutionary Conservation and Disruption in Disease.* Trends Endocrinol Metab, 2020. **31**(4): p. 320-329.

86. Okawa, H., et al., *ATP consumption by mammalian rod photoreceptors in darkness and in light.* Curr Biol, 2008. **18**(24): p. 1917-21.

87. Goldberg, A.F., *Role of peripherin/rds in vertebrate photoreceptor architecture and inherited retinal degenerations.* Int Rev Cytol, 2006. **253**: p. 131-75.

88. Matthews, H.R., et al., *Light adaptation in cone photoreceptors of the salamander: a role for cytoplasmic calcium.* J Physiol, 1990. **420**: p. 447-69.

89. Burkhardt, D.A., *Light adaptation and photopigment bleaching in cone photoreceptors in situ in the retina of the turtle.* J Neurosci, 1994. **14**(3 Pt 1): p. 1091-105.

90. Ames, A., 3rd, *CNS energy metabolism as related to function.* Brain Res Brain Res Rev, 2000. **34**(1-2): p. 42-68.

91. Birol, G., et al., *Oxygen distribution and consumption in the macaque retina.* Am J Physiol Heart Circ Physiol, 2007. **293**(3): p. H1696-704.

92. Rungger-Brandle, E., H. Kolb, and G. Niemeyer, *Histochemical demonstration of glycogen in neurons of the cat retina.* Invest Ophthalmol Vis Sci, 1996. **37**(5): p. 702-15.

93. Pfeiffer, B., et al., *Immunocytochemical demonstration of glycogen phosphorylase in Muller (glial) cells of the mammalian retina.* Glia, 1994. **12**(1): p. 62-7.

94. Coffe, V., R.C. Carbajal, and R. Salceda, *Glycogen metabolism in the rat retina.* J Neurochem, 2004. **88**(4): p. 885-90.

95. Kur, J., E.A. Newman, and T. Chan-Ling, *Cellular and physiological mechanisms underlying blood flow regulation in the retina and choroid in health and disease.* Prog Retin Eye Res, 2012. **31**(5): p. 377-406.

96. Zorov, D.B., et al., *Lessons from the Discovery of Mitochondrial Fragmentation (Fission): A Review and Update.* Cells, 2019. **8**(2).

97. Dyer, M.A. and C.L. Cepko, *p27Kip1 and p57Kip2 regulate proliferation in distinct retinal progenitor cell populations.* J Neurosci, 2001. **21**(12): p. 4259-71.

98. Dyer, M.A. and C.L. Cepko, *Control of Muller glial cell proliferation and activation following retinal injury.* Nat Neurosci, 2000. **3**(9): p. 873-80.

99. Rueda, E.M., et al., *The Hippo Pathway Blocks Mammalian Retinal Muller Glial Cell Reprogramming.* Cell Rep, 2019. **27**(6): p. 1637-1649 e6.

100. Mitra, K., et al., *A hyperfused mitochondrial state achieved at G1-S regulates cyclin E buildup and entry into S phase.* Proc Natl Acad Sci U S A, 2009. **106**(29): p. 11960-5.

101. Schieke, S.M., J.P. McCoy, Jr., and T. Finkel, *Coordination of mitochondrial bioenergetics with G1 phase cell cycle progression.* Cell Cycle, 2008. **7**(12): p. 1782-7.

102. Iwata, R., P. Casimir, and P. Vanderhaeghen, *Mitochondrial dynamics in postmitotic cells regulate neurogenesis.* Science, 2020. **369**(6505): p. 858-862.

103. Deng, Q., et al., *Cross-Talk Between Mitochondrial Fusion and the Hippo Pathway in Controlling Cell Proliferation During Drosophila Development.* Genetics, 2016. **203**(4): p. 1777-88.

104. Goldman, D., *Muller glial cell reprogramming and retina regeneration.* Nat Rev Neurosci, 2014. **15**(7): p. 431-42.